A Targeted Protein Degradation Cell-Based Screening for Nanobodies Selective toward the Cellular RHOB GTP-Bound Conformation

Nicolas Béry, Laura Keller, Marjorie Soulié, Rémi Gence, Anne-Laure Iscache, Julia Cherier, Stéphanie Cabantous, Olivier Sordet, Isabelle Lajoie-Mazenc, Jean-Denis Pedelacq, et al.

CellPress

Cell Chemical Biology
Article

A Targeted Protein Degradation Cell-Based Screening for Nanobodies Selective toward the Cellular RHOB GTP-Bound Conformation

Nicolas Bery,[1] Laura Keller,[1,2] Marjorie Soulié,[1] Rémi Gence,[1] Anne-Laure Iscache,[1,2] Julia Cherier,[1,2] Stéphanie Cabantous,[1] Olivier Sordet,[1] Isabelle Lajoie-Mazenc,[1] Jean-Denis Pedelacq,[3] Gilles Favre,[1,2,*] and Aurélien Olichon[1,4,*]

[1]Centre de Recherche en Cancérologie de Toulouse (CRCT), INSERM, Université de Toulouse, CNRS, UPS, Toulouse, France
[2]Département de Biologie, Institut Claudius Regaud, Toulouse, France
[3]Institut de Pharmacologie et de Biologie Structurale, Université de Toulouse, CNRS, UPS, Toulouse, France
[4]Lead Contact
*Correspondence: jean-denis.pedelacq@ipbs.fr (J.-D.P.), gilles.favre@inserm.fr (G.F.), aurelien.olichon@inserm.fr (A.O.)
https://doi.org/10.1016/j.chembiol.2019.08.009

SUMMARY

The selective downregulation of activated intracellular proteins is a key challenge in cell biology. RHO small GTPases switch between a guanosine diphosphate (GDP)-bound and a guanosine triphosphate (GTP)-bound state that drives downstream signaling. At present, no tool is available to study endogenous RHO-GTPinduced conformational changes in live cells. Here, we established a cell-based screen to selectively degrade RHOB-GTP using F-box-intracellular single-domain antibody fusion. We identified one intracellular antibody (intrabody) that shows selective targeting of endogenous RHOB-GTP mediated by interactions between the CDR3 loop of the domain antibody and the GTP-binding pocket of RHOB. Our results suggest that, while RHOB is highly regulated at the expression level, only the GTP-bound pool, but not its global expression, mediates RHOB functions in genomic instability and in cell invasion. The F-box/intrabody-targeted protein degradation represents a unique approach to knock down the active form of small GTPases or other proteins with multiple cellular activities.

INTRODUCTION

RHOB, a RAS-related member of the RHO family of GTPases, switches from an inactive guanosine diphosphate (GDP)-bound to an active guanosine triphosphate (GTP)-bound form that recruits effector proteins (Etienne-Manneville and Hall, 2002). RHOB's closest homologs RHOA and RHOC in their GTP-bound form are mostly localized at the plasma membrane to switch on canonical pathways regulating acto-myosin cytoskeleton (Ridley, 2006). RHOA and RHOC are mainly considered as protumorigenic in various cancers (Pillé et al., 2005; Zandvakili et al., 2017). In contrast, RHOB expression is downregulated in cancers (Adnane et al., 2002; Bousquet et al., 2009; Ju and Gilkes, 2018; Mazieres et al., 2004). This downregulation can be related to its role in promoting DNA double-strand break repair (Mamouni et al., 2014), or also in stimulating apoptosis (Couderc et al., 2008; Huang and Prendergast, 2006; Vega and Ridley, 2008; Wang et al., 2014). Moreover, RHOB is a peculiar GTPase that exerts pleiotropic functions (Vega and Ridley, 2018), and displays different levels of regulation of its expression and multiple cellular localizations (Baron et al., 2000; Fritz et al., 1995; Marcos-Ramiro et al., 2016; Sandilands et al., 2004), which may explain its dual role in cancer development and progression (Ju and Gilkes, 2018; Zandvakili et al., 2017). Indeed, depending on the cellular context, RHOB can either promote migration and invasion of cancer cells (Alfano et al., 2012; Yoneda et al., 2010) or inhibit them (Connolly et al., 2010; Zhou et al., 2011). RHOB expression also induces endothelial cell migration and vascularization (Howe and Addison, 2012). Furthermore, in the context of therapy targeting either mutated epidermal growth factor receptor (EGFR) in lung cancer (Calvayrac et al., 2017) or mutated BRAF in cutaneous melanoma (Delmas et al., 2015), RHOB expression contributes to the resistance to these treatments, confirming its paradoxical role in cancer. At the cellular level, RHOB is localized to the endosome where it regulates trafficking of the EGFR (Gampel et al., 1999; Lajoie-Mazenc et al., 2008), but nuclear RHOB is involved in angiogenesis regulation (Gerald et al., 2013). Although RHOB expression is regulated by mRNA stabilization or regulation of protein turnover (Kovačević et al., 2018), the molecular mechanisms of the multiple cellular activities of RHOB remain largely unknown.

Cellular functions of small GTPases of the RHOA/B/C subfamily have been assigned using well-characterized cell biology tools. For instance, the Q63L mutant locked in a conformation mimicking the GTP-bound RHO or the dominant negative T19N variant (Schaefer et al., 2014; Subauste et al., 2000) (hereafter named RHO L63 and RHO N19, respectively) were used to study the functions of RHO. Heterologous expression of fluorescence resonance energy transfer (FRET) biosensors (Pertz and Hahn, 2004; Reinhard et al., 2016), or inactivation of multiple endogenous RHOs through ADP-ribosylation by C3 toxin treatment (Aktories et al., 1992), are other tools used in RHO cell biology. Moreover, pharmacological inhibition of

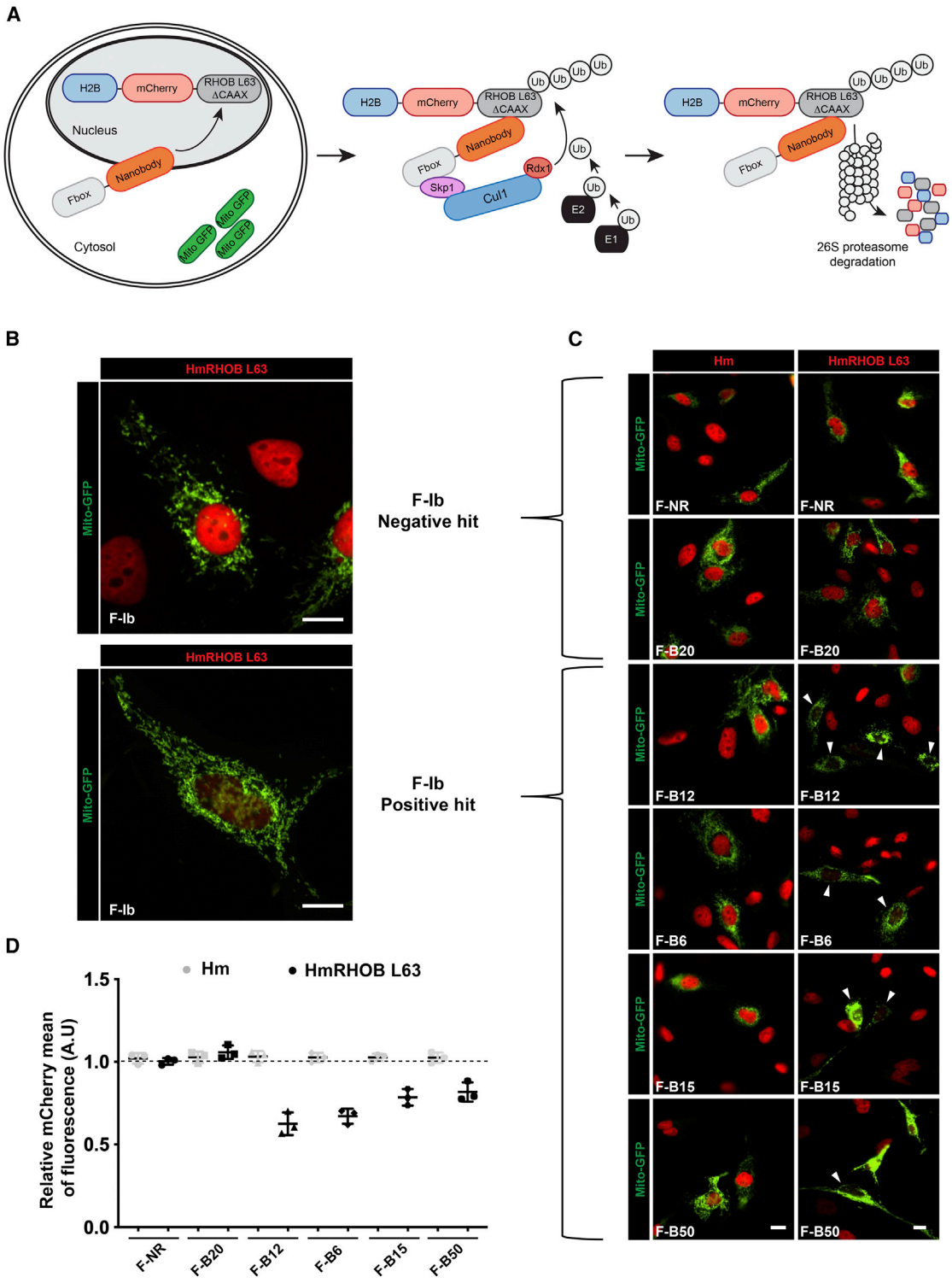

Figure 1. Cell-Based Screen of Degrading Intrabodies

The screen was performed in the H2882 H2B-mCherry-RHOB L63 cell line (HmRHOB L63). Three hundred F-box-Ib clones were expressed from a bicistronic vector also encoding a mitochondrial targeted monomeric GFP. Forty-eight hours after transfection, evaluation of the nuclear red fluorescence level was performed in transfected cells identified by GFP-labeled mitochondria (green, Mito-GFP). Then, the positive hits were further counter-selected in an H2882 control cell line H2B-mCherry (designated Hm).

(A) Scheme of the protein interference screen based on F-Ib. When the Ib domains are able to interact specifically with H2B-mCherry-RHOB L63, allowing the F-box domain to recruit the Skip1 (Skp1)-Cullin1 (Cul1)-F-box (SCF) complex to the targeted antigen, H2B-mCherry-RHOB is degraded by the 26S proteasome.

(legend continued on next page)

RHO-GTPases has emerged through structure-based docking screening strategies leading to compounds that are not isoform selective (Shang et al., 2012, 2013). So far, the only selective approaches include small interfering RNA (siRNA)-induced protein downregulation (Alfano et al., 2012; Bousquet et al., 2009; Vega et al., 2012), CRISPR/Cas9 gene invalidation in cell lines (Sebestyen et al., 2016), and the development of knockout mouse models (Bustelo et al., 2007; Heasman and Ridley, 2008). Nevertheless, downregulating a single RHO of the RHOA/B/C subfamily often induces an upregulation of one or the two other members (García-Mariscal et al., 2017; Guilluy et al., 2011; Ho et al., 2008; Stultiens et al., 2012; Vega et al., 2011), which may indicate the occurrence of additional cellular compensation mechanisms or the masking of some phenotypes. Despite the fact that RHO's conformational switch leads to distinct cellular pools of GTP- and GDP-bound RHO proteins, RHO inhibition at the RNA or DNA level downregulates the expression level of both fractions. At present, assignment of RHOB protein functions relative to its GTP-bound pool remains elusive, and its specific effectors are not clearly identified, mainly in the regulation of cell motility or in genomic instability (Vega and Ridley, 2018). Therefore, more selective tools are needed to formally decipher the role of RHOB-GTP and the resulting cell signaling mechanisms.

Selective inhibition of intracellular protein activities is a persistent challenge in cell biology. Several methods that specifically deplete endogenous proteins in cells were developed, such as the targeted degradation induced by small-molecule chimera called PROTAC (Raina and Crews, 2017), by microinjected antibodies (Clift et al., 2017), or by intracellular antibodies (also called intrabodies or Ibs) (Guglielmi and Martineau, 2009; Joshi et al., 2012; Kaiser et al., 2014). Taking advantage of the specificity of domain antibodies to their target, protein interference strategies often involve domains that recruit a ubiquitin ligase to efficiently degrade the intracellular antigen by the proteasome machinery (Caussinus et al., 2011; Kuo et al., 2011; Melchionna and Cattaneo, 2007). These approaches are well suited for selectively degrading activated pools of the target protein, a strategy that is not possible using DNA- or RNA-targeting methods. We previously isolated nanobodies from the NaLi-H1 library, a phage display library of humanized synthetic single-domain antibodies, and demonstrated the functionalization of anti-GFP Ibs by an amino-terminal fusion to an F-box domain (Moutel et al., 2016).

In this study, we engineered an analytical tool based on an F-box-fused single-domain intrabody (F-Ib) to selectively degrade the GTP-bound form of endogenous RHOB. To achieve this goal, we enriched a phage display library with nanobodies that bind to RHOB-GTP, and developed a cell-based assay to screen the protein degradation of antigen/F-Ib complexes. Using this strategy, we identified several Ibs that recognize RHO-GTP proteins, and characterized one nanobody that showed greater selectivity to RHOB-GTP. Here, we demonstrate that the active GTP-bound state of RHOB is responsible for the regulation of genome stability and migration and invasion of human bronchial cells. Altogether, our data highlight the relevance of this molecular tool to investigate the cellular functions of RHOB-GTP in various models.

RESULTS

Cell-Based Screen of Intrabodies Targeting RHOB-GTP

Starting with the NaLi-H1 large synthetic library (Moutel et al., 2016), we selected nanobodies that recognize the native conformation of RHOB-GTP using a subtractive phage display selection protocol (Chinestra et al., 2012). A competitive selection was carried out *in vitro* by pre-clearing steps in the presence of an excess of GDP-loaded wild-type RHOB, as well as the constitutively active GTP-bound RHOA L63 and RHOC L63 mutants to deplete nanobodies cross-reacting within RHOA and RHOC, respectively (Figure S1). Although functionalization of anti-GFP nanobodies through the SlmbF-box fusion was successfully reported (Caussinus et al., 2011), it also failed for other nanobodies (Moutel et al., 2016). Therefore, we set up a cell-based screen to directly select intrabodies that enabled targeted protein degradation (Figure 1A), referred to as F-Ib (method outlined in Figure S1). The target consists in a CAAX box-deleted RHOB L63, N-terminally fused to the mCherry fluorescent protein (Figure 1A). To avoid potential cellular toxicity of RHOB L63 mutant, histone H2B domain was C-terminally fused to mCherry-RHOB L63 to localize this construct to the chromatin, where it showed no sign of perturbation (Figures 1B and S1). This strategy allowed us to successfully monitor H2B-GFP degradation using anti-GFP F-Ib (Moutel et al., 2016). The H2B-mCherry-RHOB L63 chimera construct was then expressed in the *RHOB*$^{-/-}$ lung epithelial tumor H2882 cell line (Sato et al., 2007) to generate a stable cell line, named HmRHOB L63.

The cell-based screening of F-Ibs was performed after subcloning of the pool of nanobodies enriched against RHOB-GTP during the four rounds of phage display into a bicistronic vector. The first cistron expresses the F-Ib tagged downstream with 6xHis and Myc tags, while the second cistron expresses a GFP targeted to mitochondria (Mito-GFP) (see the STAR Methods, Figures 1 and S1). We then monitored, using fluorescence

(B) The positive hits correspond to HmRHOB L63 cells harboring GFP in mitochondria and a strong decrease of mCherry fluorescence in the nucleus. In negative hits, the red nuclear fluorescence remains unchanged. Scale bars, 10 μm.

(C) Representative field on fixed HmRHOB L63 or Hm control cells expressing selected F-Ib. F-NR is a non-related Ib used as negative control and F-B20 is representative of all negative hits, whereas F-B6, F-B12, F-B15, and F-B50 are the four strongest positive hits. Arrowheads indicate positive cells for antigen-targeted degradation. Scale bars, 10 μm.

(D) Protein interference evaluation by mCherry fluorescence quantification by flow cytometry in Hm and HmRHOB L63 cell lines. mCherry fluorescence was quantified in the transfected GFP-positive subpopulation and in the non-transfected GFP-negative subpopulation for each F-Ib. The ratio of each mean of fluorescence (transfected versus non-transfected population) gives a relative mCherry fluorescence intensity for each F-Ib, then normalized to the F-NR one. Mean ± SD is represented with all the biological repeats as dots (n = 3 biological repeats).

See also Figure S1.

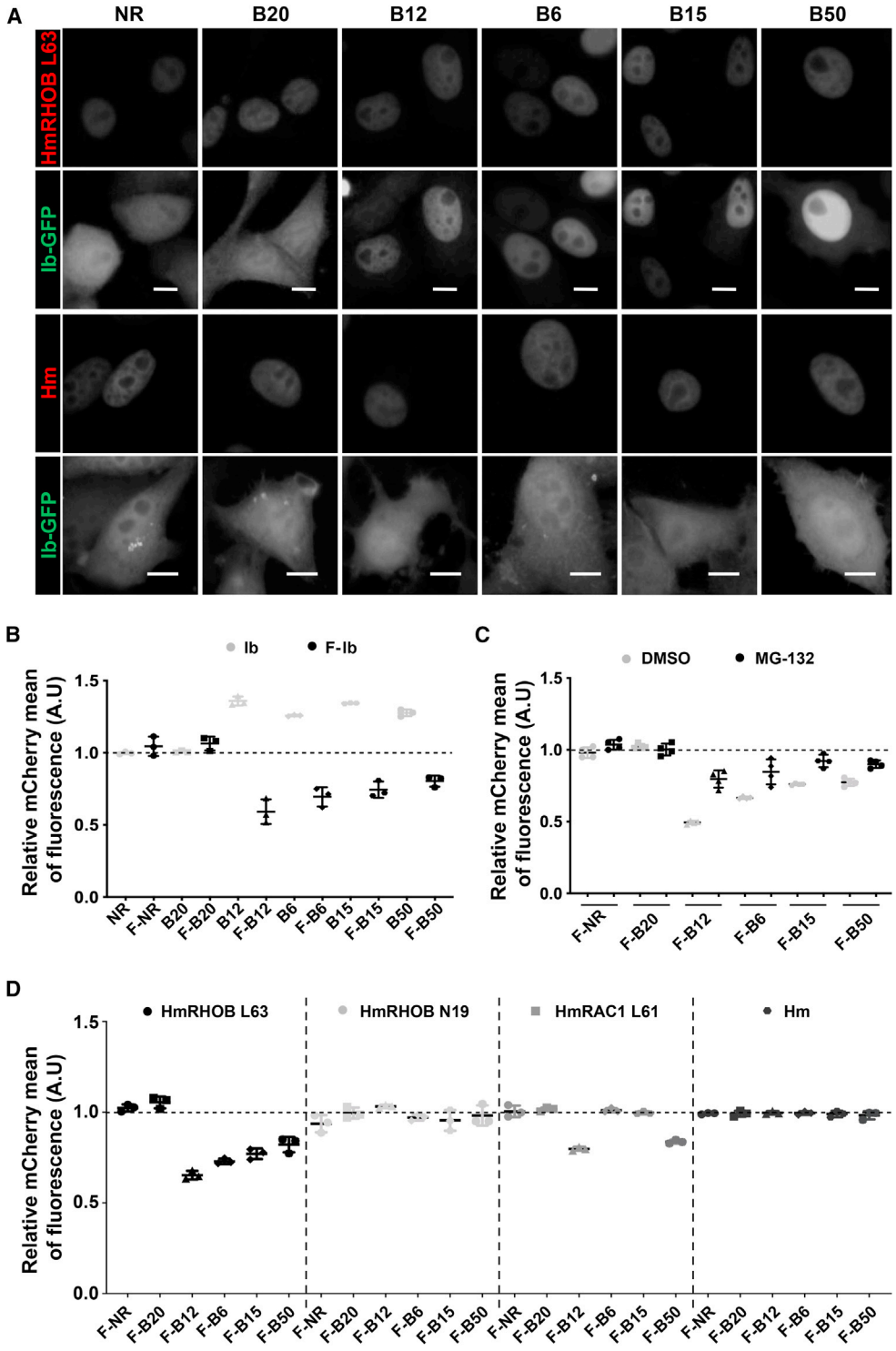

Figure 2. Functionality and Selectivity of Intrabodies on Heterologous Target Antigens

(A) Ibs-GFP were co-transfected in HeLa S3 cells with the nuclear constructs H2B-mCherry-RHOB L63 (HmRHOB L63) or H2B-mCherry (Hm). Scale bars, 10 μm.

(B) F-Ib or Ib were transfected in HmRHOB L63 cell line. Quantification of the mCherry fluorescence by flow cytometry shows only a decrease of fluorescence with the positive F-Ibs and not with the Ibs.

(C) HmRHOB L63 cells were transfected with F-Ib and treated for 36 h with 1 μM MG132 (a proteasome inhibitor) or DMSO and then the mCherry fluorescence was quantified by flow cytometry.

(legend continued on next page)

microscopy, the decay of the mCherry nuclear fluorescence in cells showing green fluorescent mitochondria (Figures 1 and S1). As a negative control, we included an unrelated nanobody originating from the same library (hereafter named NR for non-RHO). Three hundred clones were randomly picked, named B1 to B300, and transiently transfected into the HmRHOB L63 cell line. Only 30 F-Ibs induced a drastic decrease of mCherry fluorescence in the nuclei of Mito-GFP-positive cells (Figure 1B). Sequencing of theses clones revealed that they correspond to only eight different nanobodies. Of them, four clones, F-B6, F-B12, F-B15, and F-B50, were over-represented and, hence, were selected for further characterization (Figure 1C). The F-B12 clone corresponds to the nanobody previously isolated as a pan RHO/RAC-GTP binder from NaLi-H1 library (Moutel et al., 2016). In the negative clones, no apparent decrease of fluorescence was observed in any transfected cells, and their sequences revealed that one of them, referred to as B20, was present in nearly half of the picked clones (Figure 1C). Next, we counter-selected the positive hits in a control H2882 cell line stably expressing H2B-mCherry construct (hereafter named Hm). We showed that these hits did not decrease the mCherry fluorescence in that cell line (Figure 1C). Finally, we quantified the degradation effectiveness of the four selected F-Ibs by quantitative flow cytometry within GFP-positive cells. The four positive clones targeted RHOB as they induced at least a 25% decrease of the mCherry fluorescence in HmRHOB L63 cells but not in Hm cells (Figure 1D). In summary, this original cell-based screen identified four F-Ib-degrading H2B-mCherry-RHOB L63 chimera.

Characterization of Conformational Selectivity of Intrabodies

Next, we tested whether the selected intrabodies could localize to the same subcellular compartment as the antigen. We fused the nanobody moiety to the GFP and co-transfected into HeLa S3 cell line the Ib-GFP with a plasmid expressing the HmRHOB L63 or the Hm constructs. We observed a nuclear localization for B50, B6, B12, and B15 Ib-GFP in the RHOB L63-expressing cells, while a diffuse staining was observed in H2B-mCherry control cells (Figure 2A).

We performed flow cytometry quantification of mCherry fluorescence in the HmRHOB L63 cell line to determine whether the degradation was F-box dependent. We did not observe a decrease in mCherry fluorescence upon transfection of intrabodies lacking the F-box, but rather an increase of fluorescence when expressing positive hits in comparison with negative binders (Figure 2B). This fluorescence may be explained by the fact that intrabodies and their target antigens form complexes with a longer half-life (Tang et al., 2016). We further confirmed that the fluorescence decay was dependent on the proteasome using the proteasome inhibitor MG132 (Figure 2C). Altogether, these results demonstrate that the F-Ibs target the nuclear RHOB L63 chimera and degrade it through the proteasome.

To assess the selectivity of F-Ib-positive hits toward the RHO-GTP conformation, we generated a stable H2882 cell line expressing the H2B-mCherry-RHOB N19 dominant negative mutant (Farnsworth and Feig, 1991; Lajoie-Mazenc et al., 2008). Transfection of the selected F-Ibs in this HmRHOB N19 cell line did not induce any fluorescence decay, suggesting that all four positive hits were selective toward the RHOB L63 mutant (Figure 2D). Furthermore, this result was confirmed by the absence of nuclear localization of Ib-GFP when co-expressed with HmRHOB N19 in HeLa S3 cells for which co-transfection was more efficient than in H2882 cells (Figure S2A).

We then engineered a stable H2882 cell line expressing an H2B-mCherry-RAC1 L61 GTP-bound mimetic mutant deleted for the CAAX prenylation box (hereafter designated HmRAC1 L61) to evaluate whether F-Ibs cross-react with the closely related RAC subfamily (Wennerberg and Der, 2004). Among the positive hits, F-B50 and F-B12 caused a significant decrease in the fluorescence level of HmRAC1 L61 cells, whereas F-B6 and F-B15 did not degrade RAC1 L61 (Figure 2D). Accordingly, we only observed a selective nuclear localization of Ib-GFP for the B12 and B50 in HmRAC1 L61-expressing HeLa S3 cells (Figure S2B). These data suggest that the most selective Ibs toward RHOB L63 compared with RAC1 L61 are the B15 and B6 clones.

Because B6 showed more efficiency in degrading RHOB L63 than B15 (Figures 1D and 2), we then studied the selectivity of B6 Ib toward the RHOA/B/C subfamily and compared it with the pan RHO B12 (Moutel et al., 2016). The production of stable cell lines expressing chromatin-anchored RHOA or RHOC L63 failed, therefore we transiently co-transfected bait and prey into HeLa S3 cells. Expression of H2B-mCherry-RHO L63 with Ib-GFP induced visually a complete nuclear localization of B12. Quantification of the nuclear and cytoplasmic GFP fluorescence signals showed that the faint signal measured into the cytoplasm corresponds to 20% of the whole-cell fluorescence intensity (Figure S3). B6-GFP showed similar nuclear fluorescence in cells expressing RHOB L63 chimera. However, higher cytoplasmic signal correlated with a more diffused nucleo-cytoplasmic pattern was measured in cells expressing nuclear RHOA L63 or RHOC L63, indicating a lower nuclear relocalization of the B6-GFP compared with cells expressing the chimera RHOB L63 (Figure S3). These results suggest a stronger selectivity of the B6 Ib toward RHOB-GTP compared with RHOA/C-GTP and RAC1-GTP, and led us to pursue the characterization of this Ib.

B6 Nanobody Is Specific to the GTP-Bound RHOB Conformation

To evaluate the ability of B6 to selectively immunoprecipitate RHOB-GTP, we expressed it N-terminally fused to a 6xHis tag for Ni-NTA capture. After 24 h of Ib transient transfection in HeLa S3, we performed pull-down assays on a cell lysate containing RHO-GTPases with either non-hydrolysable GTPγS or GDP. B6 immunoprecipitated RHOB from cell lysates when GTPases were loaded with GTPγS but not with GDP (Figure 3A), indicating that B6 specifically binds the GTP-bound form of RHOB. Next, we assessed the interaction of intrabodies with

(D) F-Ib were transfected in Hm, HmRHOB L63, and HmRHOB N19 cell lines, and mCherrry fluorescence was evaluated by flow cytometry. The relative mCherry fluorescence intensity of each F-Ib/Ib was averaged and normalized to F-NR/NR ones as described in Figure 1. Mean ± SD is shown with all the biological repeats displayed as dots (n = 3 biological repeats).
See also Figures S2 and S3.

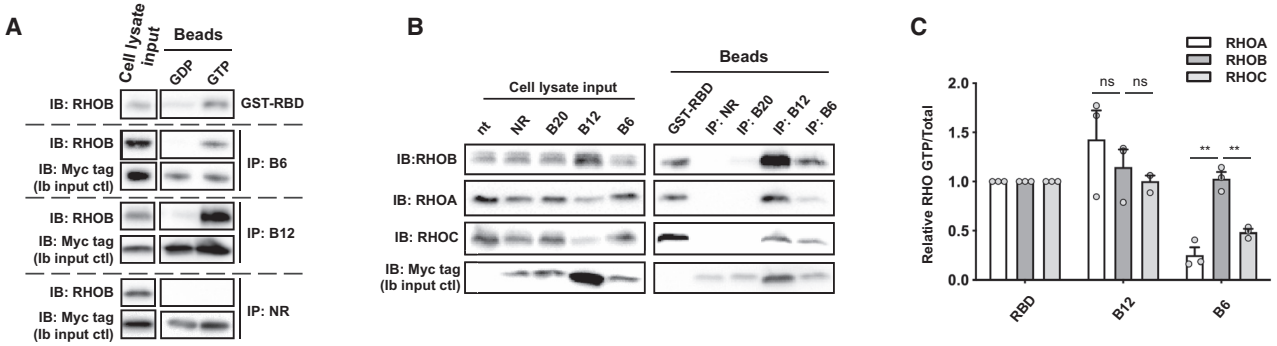

Figure 3. Specificity and Conformational Selectivity of the B6 Intrabody toward Endogenous RHOB-GTP

(A) Twenty-four hours after Ibs transfection in HeLa S3 cells, RHO-GTPases were loaded separately with GDP and GTPγS in the cell lysates. Then Ibs were precipitated by Ni-NTA beads. The level of RHOB-GDP and RHOB-GTPγS bound to the Ib was revealed with an anti-RHOB antibody. The GST-RBD pull-down was used as a positive control and the quantity of Ib pulled down by Ni-NTA beads revealed by myc antibody. No signal was detectable for RHOB on the beads immunoprecipitate of the NR condition at the exposure time of the representative blot.

(B) HeLa S3 cells were transfected for 24 h with Ib-expressing plasmids. Co-immunoprecipitation of His tag intrabodies was compared with GST-RBD pull-down as control to reveal the cellular level of RHO-GTP (beads). The total level of RHO proteins was revealed by loading 2% of input (input). Ib production is shown with myc tag revelation and tubulin is the loading control.

(C) Quantification of three independent intrabody co-immunoprecipitation experiments. The relative activity was calculated as the ratio between GTP level and input level. The relative activity was normalized to the GST-RBD pull-down assay. Normalized means ± SEM are shown (n = 3 biological repeats). ns: non-significant, **$p < 0.01$.

the endogenous RHO-GTP fraction. Figures 3B and 3C show that the B12 pan RHO-GTP captured the GTP-bound fraction of RHOA, RHOB, and RHOC in a range similar to that of the standard RHO-binding domain of the RHOTEKIN effector (GST-RBD beads) on cell extract (Ren et al., 1999). In contrast, the B6 Ib efficiently co-precipitated RHOB-GTP, but to a lesser extend RHOA-GTP and RHOC-GTP. Taken together, these results suggest a preferential binding of the B6 Ib toward the endogenous RHOB-GTP conformation.

Crystal Structure of the RHOB-GTP/B6 Complex

To gain insights into RHOB recognition by the nanobody B6, we first co-purified B6 with GTP-bound RHOB L63 missing the last 11 amino acids involved in membrane anchoring. We then solved the three-dimensional structure of the complex by X-ray crystallography at a resolution of 1.5 Å and compared it with the X-ray structure of RHOB-GTP alone (see statistics in Table S1). The RHOB-GTP/B6 interface buries ~700 $Å^2$ of highly complementary surfaces (Figure 4A). The GTP is located in an electropositive pocket at the interface between RHOB and B6 within hydrogen bonding distance of the side chain amide of N113 of the CDR3 loop, a major contributor to the interface (Figures 4B and 4C). Additional polar interactions involving the exposed CDR3 loop include the side chains of Q106 and Y114 with Y34 from RHOB (Figure 4C).

One remarkable feature is the polar network formed by residues H126, E130, and R133 of the RHO insert helix, at hydrogen bond distance to T94 and Y96 from strand β7 and the main chain atoms of W115 and G118 downstream of the CDR3 loop (Figure 4C). In addition, stacking interactions via the indole ring of W112 from CDR3 may also contribute to the stabilization of the helix. The sequence of the RHO insert helix of RHOB differs from that of RHOA and RHOC isoforms at amino acid positions 127, 129, and 133. Residues V127 and T129 in RHOB do not interact directly with the CDR3 loop of B6. Superimposition of the GTP-bound structures of RHOB alone and in complex with B6 highlights some significant changes in the positioning of the RHO insert helix accompanied with a reorientation of the side chains of E130 and R133 (Figure 4D). Therefore, the side chain of E130 in the complex finds itself in an orientation favorable for interactions with residues Y96 and G118 of B6 (Figure 4C). A reorientation of the imidazole group of H126 is also observed that favors interactions with the carbonyl group of W115 of B6. In conclusion, specific interaction networks between B6 and RHOB-GTP, along with an optimized surface shape and charge complementarity, provide good evidence for the conformational selectivity of B6 toward the active form of RHOB.

To get insights into the potential B6/RHOB selectivity *in vitro*, affinity measurements on purified recombinant B6 domain antibody and RHO isoforms were performed by SPR (see the STAR Methods). RHO isoforms include RHOB loaded with GTPγS or GDP, the L63 active mutants of RHOA, RHOB, and RHOC, and the dominant negative RHOB mutant N19. As expected, no resonance unit was measured for RHOB N19 (Figure S4). The K_D value of 30.8 ± 2 nM measured for RHOB L63 is approximately 3 and 6 times lower than that of RHOA L63 and RHOC L63, respectively (Figure S4). The mutation of the Arg at position 133 of RHOB into a Lys, as found in RHOA or RHOC, led to K_D values of 50.7 ± 1.1 nM, suggesting that this residue may also contribute to the selectivity toward RHOB. Altogether, these results show a higher affinity of the B6 domain toward RHOB-GTP *in vitro*.

F-B6 Allows Selective Protein Degradation of Endogenous RHOB-GTP

B6 nanobody exhibits a higher affinity for RHOB-GTP than RHOA-GTP and RHOC-GTP *in vitro*, and a selectivity toward endogenous RHOB-GTP *in cellulo*. With the aim of inhibiting selectively RHOB-GTP, we investigated whether F-B6 could degrade the endogenous RHOB-GTP in HeLa S3 cells. Protein interference was quantified by GST-RBD pull-down from cells

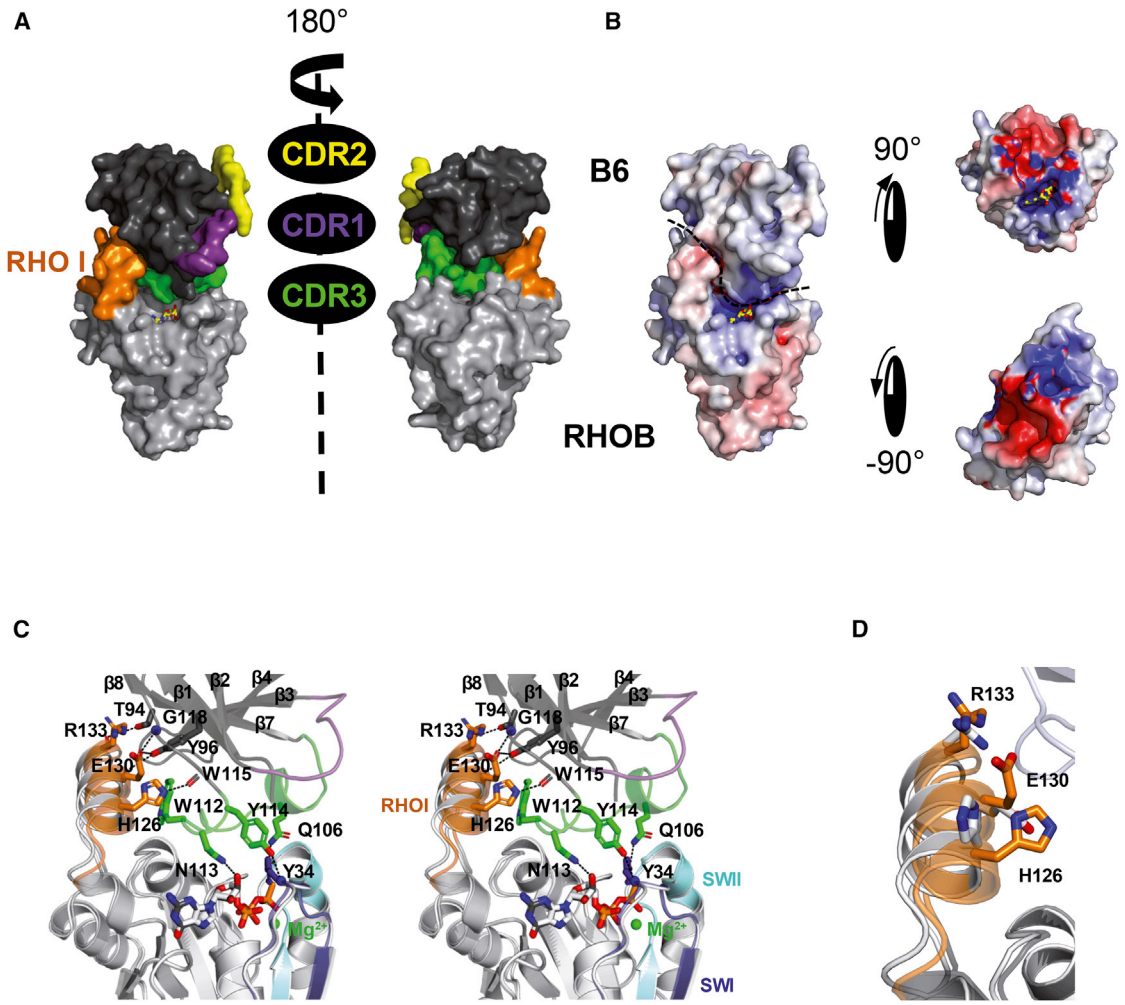

Figure 4. B6 Nanobody Interaction with RHOB L63-GTP

(A) Surface representation of the interactions between RHOB (gray) and B6 (black) displayed in two orientations. The RHO insert helix (RHOI) is colored orange. The loops CDR1, CDR2, and CDR3 of B6 are colored purple, yellow, and green, respectively. GTP is shown as sticks, with nitrogen and oxygen atoms in blue and red, respectively.

(B) Molecular surface mapped with calculated vacuum electrostatic potential. Blue shading (+10 k_BT/e) indicates electropositive and red shading (−10 k_BT/e) indicates electronegative protein surfaces. Rotation of RHOB-GTP and B6 by 90° to visualize electrostatic pairing (right). Electrostatic potential surface calculations with PyMol (The PyMOL Molecular Graphics System, version 2.0 Schrödinger) using APBS as the macromolecular electrostatics calculation program (Baker et al., 2001).

(C) Ribbon stereoview representation detailing the interactions at the contact interface viewed in the same orientation as in left. Interactions involve residues from the switch loop I (SWI) (dark blue), the RHO insert helix (orange), and the CDR3 loop (green). A bound Mg^{2+} ion is shown as a green sphere. Orientation is the same as in (A, left).

(D) Close-up view of the RHO insert helix after superimposition of RHOB-GTP alone (white) on its counterpart in the RHOB-GTP/B6 complex (orange).

See also Table S1 and Figure S4.

transfected with F-Ibs (Figure 5). We observed that F-B6 induced a significant downregulation of RHOB-GTP but not of RHOA-GTP or RHOC-GTP (Figures 5A and 5B). Unlike RHOB siRNA that significantly increased RHOA expression in this cell line (Figures S5A and 5B), no significant change on RHOA expression was observed upon expression of F-B6 (Figure 5A). This result suggests a specific downregulation of RHOB-GTP by F-B6 without any compensation mechanisms on RHOA and RHOC expression. In contrast, F-B12-mediated efficient degradation of multiple RHO-GTP was associated with a strong upregulation of total RHOB level (Figure 5A), indicating that the broad downregulation of RHO/RAC-GTP induces a compensatory mechanism between these GTPases.

Next, we assessed the efficiency of the F-Ib interference on the physiological stimulation of RHO activity by growth factors (Gampel et al., 1999). After 24 h of serum starvation, the RHOA/B/C GTP-bound fraction increased upon EGF stimulation and reached a maximum from 5 to 30 min (Figure S5C). Analysis of F-Ib effect after 15 min of EGF treatment showed that F-B6 impeded strongly RHOB-GTP cellular induction, while F-B12 prevented this stimulation for all three RHO-GTPases, and F-NR or F-B20 controls had no effect (Figures 5C, 5D,

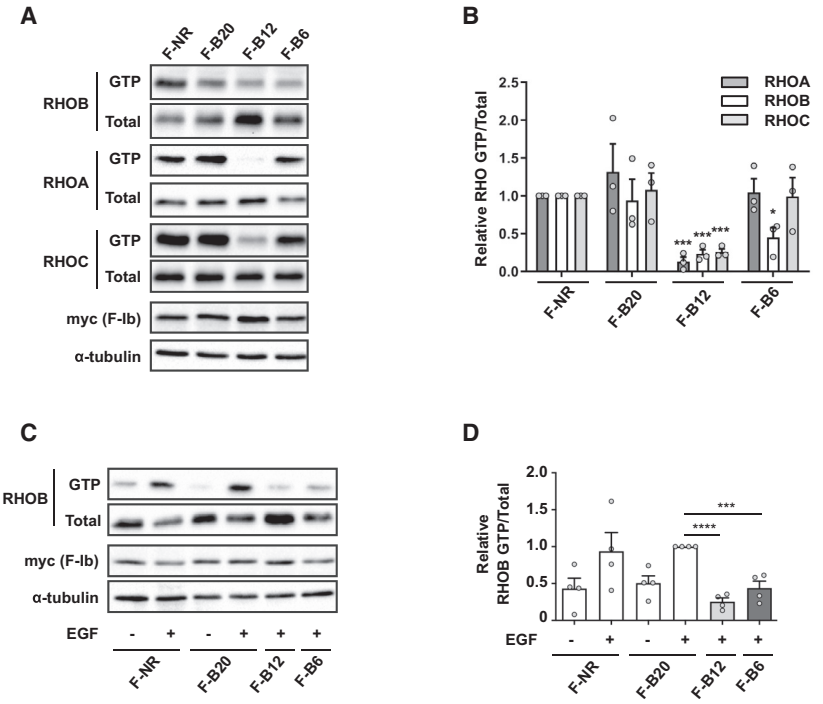

Figure 5. Endogenous RHOB-GTP Activity Knockdown

(A) Basal endogenous RHOB activity knockdown. A GST-RBD pull-down was performed for each F-Ib to control RHO-GTP level (lines RHOB-GTP, RHOA-GTP, and RHOC-GTP), and the total level of RHO proteins was revealed by loading 2% of input (lines total RHOB, total RHOA, and total RHOC). F-Ib production is shown with myc tag revelation and tubulin is the loading control.

(B) Quantification of three independent GST-RBD pull-down experiments. The relative activity was calculated as the ratio between GTP to input levels normalized to tubulin by densitometry measurements. The relative activity was normalized to the relative amount quantified from the cells transfected with the F-NR. Normalized means ± SEM of three independent experiments are shown. *$p < 0.05$, ***$p < 0.001$.

(C) Inhibition of endogenous RHOB activation induced by EGF treatment. HeLa S3 cells were transfected for 48 h with F-Ib including 24 h of serum starvation. Then cells were treated for 15 min by EGF, and the RHOB-GTP level was checked by GST-RBD pull-down.

(D) Quantification of (C) calculated as in (B) is shown with normalized means ± SEM of three independent experiments, displayed with normalization to F-B20 + EGF condition. ***$p < 0.001$, ****$p < 0.0001$.

See also Figure S5.

and S5D–S5F). Taken together, these results illustrate the first example of a genetically encoded molecule that enables selective cellular inhibition through targeted protein degradation of endogenous RHOB-GTP.

RHOB-GTP Regulates Genome Stability and Protects from Acquisition of Invasive Phenotypes

We previously observed an accumulation of nuclear γ-H2AX foci, a DNA damage marker, following RHOB knockdown by siRNA as also found in knockout mice models (Mamouni et al., 2014; Meyer et al., 2014). To determine whether the role of RHOB in maintaining genomic stability depends on the GTP-bound fraction or on total RHOB, we compared the effect on endogenous γ-H2AX foci after F-B6-targeted degradation or siRNA-mediated knockdown of RHOB. In lung adenocarcinoma PC9 cells, siRNA-mediated RHOB knockdown induced a 46% ± 2.3% increase in the mean number of γ-H2AX foci per nucleus (Figures 6A and 6B). Quantification of the number of γ-H2AX foci in cells expressing F-B6 showed an increase of 34% ± 6.5% of γ-H2AX foci per nucleus in comparison with the F-NR control (Figures 6C and 6D). These data suggest that RHOB-GTP, but not RHOB-GDP, would be primarily responsible for the role of RHOB in maintaining genomic stability.

Global downregulation of RHOB expression induces the AKT1/RAC1 pathway, which favors invasiveness of human bronchial BEAS-2B cells (Bousquet et al., 2009, 2015). As cell motility involves an interplay between several RHO-related GTPases, we reconsidered the role of RHOB in the invasiveness of BEAS-2B cells by selectively targeting RHOB-GTP using F-B6. We tightly controlled F-B6-mediated protein degradation by lentiviral expression under the control of a doxycycline-inducible promoter (Figure S6A). To validate F-B6 selectivity in this model, we generated a control cell line that expresses F-NR, and analyzed the doxycycline dose-response effect on the level of GTP-bound RHOA/B/C. Figures S6D–S6F show, at 1 μg mL^{-1} of doxycycline, an increase of F-B6 expression correlating with a selective downregulation of RHOB-GTP, which is dependent on the proteasome activity (Figure S6G). In these conditions, both cell viability and proliferation were not affected (Figures S6B and S6C).

In this model, we examined cell migration in a Transwell system (Figures 7A–7D). After 48 h of doxycycline induction, the expression of F-B6 correlated with a 2-fold increase in cell migration, strongly suggesting that selectively inhibiting RHOB-GTP is sufficient to induce a phenotype previously associated with RHOB RNAi global knockdown (Figures 7C and 7D). Next, we evaluated whether the cell migration was related to RHOB-GTP-mediated protein degradation. To achieve this, F-Ib expression induction was stopped after 24 h by doxycycline removal, and analysis was performed at 48 h (Figures 7A–7D), when F-Ib expression levels dropped back to a non-detectable level. As a result, the number of migrating cells decreased, indicating that F-B6 extinction rescued the slower cell migration. Consistently, cells expressing F-B6 showed a marked increase in invading capacity in Matrigel (Figures 7E and 7F). Finally, in F-B6-expressing cells, AKT phosphorylation and RAC1 activation were significantly increased, showing that RHOB-GTP downregulates the AKT1/RAC1 pathway to inhibit motility (Figures 7G and 7H). Altogether, these results show that RHOB-GTP prevents the acquisition of the invasive phenotype in human bronchial cells.

DISCUSSION

Intracellular expression of single-chain fragment variable (scFv), VH/VL or nanobodies genes has already been used in a few cases to track or modulate intracellular targets (Haque et al.,

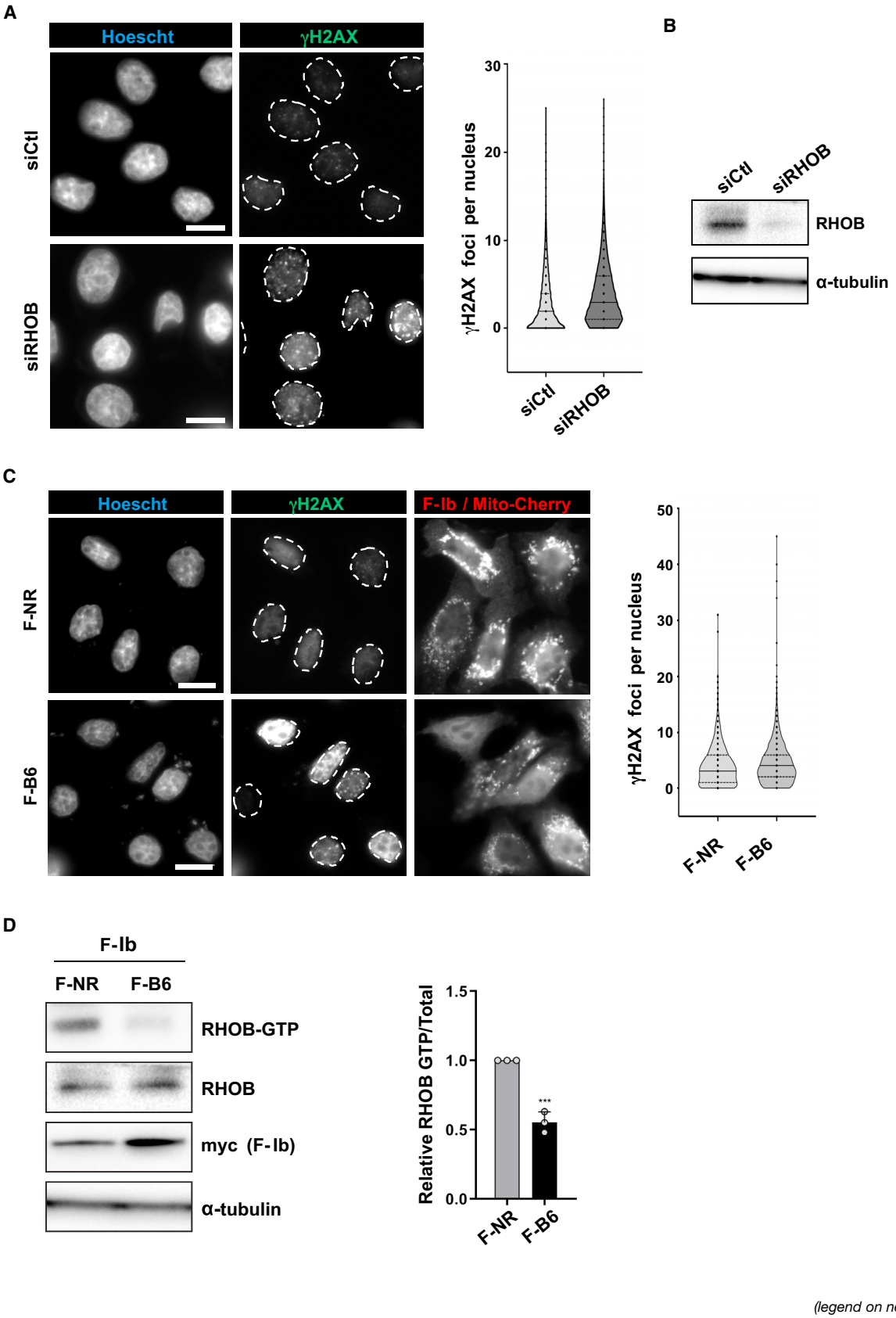

(legend on next page)

2011; Helma et al., 2015; Koo et al., 2014). The GTP-loaded conformer of small G proteins has also been targeted by intrabodies (Nizak et al., 2003; Tanaka et al., 2007). However, the production of functional intrabodies in cells relies both on the ability to recognize epitopes in the intracellular complexity and on the intrinsic stability of the antibody fragment expressed within the reducing cytosol (Joshi et al., 2012). This could partially explain why, in a previous study, we succeeded in discriminating RHOB from RHOA and RHOC *in vitro* using scFv, but we failed to use them as intrabodies (Chinestra et al., 2014). In this study, the targeted protein degradation cell-based screening discriminates positive F-Ib from non-functional F-Ib such as the B20 clone, although being enriched during the phage display. This illustrates the critical importance of the cell-based assay to identify functional F-Ib in a one-step procedure.

In addition, discriminating proteins among the subgroup of RHO is particularly challenging because RHOB shares more than 85% sequence identity with RHOA and RHOC. Even though the selection included depletion steps, most of the selected F-Ibs were pan RHO-GTP. As an example, the B12 domain antibody has nanomolar affinity toward RHOB and sub-nanomolar affinities toward RHOA/C and RAC1 (Moutel et al., 2016). However, the F-B6 targeted selectively endogenous RHOB-GTP. Consistently, X-ray crystallography revealed that the B6 domain binds to RHOB-GTP through the potential involvement of the RHOB-specific residue R133 from the RHO insert domain, while this selectivity is not only relying on the R133 residue according to *in vitro* affinity measurements. Although the selectivity between RHO isoforms appeared low *in vitro*, *in cellulo* we also observed a selectivity of the B6 nanobody alone toward RHOB-GTP. We cannot rule out the possibility that this selectivity is doped by the fused F-box domain, likewise some PROTACs small molecules conferred a selective targeted degradation compared with the parental molecules (Bondeson et al., 2018; Nowak et al., 2018; Olson et al., 2017). Finally, the specific ability of F-B6 to degrade preferentially RHOB in the cellular complexity depends on the epitope conformation and availability according to RHOB-GTP regulations.

The SImbFbox used in F-Ib constructs seemed also to be effective in preventing minute amounts of RHO activation upon growth factor stimulation, albeit this is a millisecond range process as judged by FRET biosensors studies (Pertz and Hahn, 2004; Reinhard et al., 2016). The apparent efficacy of the F-Ib even on fast cellular process, although being analyzed after 15 min treatment by EGF, depends on the high affinity of the intrabody, but also the high expression level compared with endogenous active RHOs, as well as multiple parameters related to the F-box stability itself, ubiquitin ligase component, and lysine residues on the target (Kipreos and Pagano, 2000; Skaar et al., 2013). In cell lines where RHOB activation is tightly regulated with a fast turnover, a competition between activation and targeted degradation may occur and impair the assessment of the knockdown. Conversely, F-Ib-targeted protein degradation required expression of the construct and accumulation of the protein to be efficient. However, the time range required for expression may give rise to cellular adaptation. To circumvent these limitations, the F-B6 could be further engineered to achieve a fast activation, through either chemical control, for example by expressing the F-box and the Ib separately in a chemical-inducible dimerization strategy (Goedhart and van Unen, 2017; Rakhit et al., 2014), or alternatively by using light-inducible optogenetic system (Zhang and Cui, 2015). This genetically encoded binding domain could also be engineered to reach a better signal-to-noise ratio of the bound moiety in order to visualize endogenous RHOB-GTP in real time in cells. Such approaches complementary to existing ones could be useful to identify RHOB-GTP partners.

Engineering the B6 nanobody could be particularly interesting to study whether RHOB functions rely on RHOB-GTP in various models. For instance, when the protein localizes at the plasma membrane (Vega et al., 2012, 2015), at the endosomes (Kovačević et al., 2018; Lajoie-Mazenc et al., 2008; Sandilands et al., 2004), or in the nucleus (Gerald et al., 2013; Sebestyen et al., 2016), as well as during the response to stress that induces RHOB expression and activation (Canguilhem et al., 2005; Mamouni et al., 2014; Wang et al., 2014). Notably, to investigate the dual roles of RHOB in cancer, F-B6 could be used to decipher the function of RHOB-GTP in other models, such as adaptive mechanisms of resistance to EGFR-tyrosine kinase inhibitors in non-small cell lung cancer (Calvayrac et al., 2017) and to mitogen-activated protein kinase (MAPK) inhibitors in *BRAF*-mutant melanoma (Delmas et al., 2015), or in models of angiogenesis (Gerald et al., 2013) or inflammation (Mandik-Nayak et al., 2017). Nevertheless, future work should take care of potential cellular compensation mechanism by modulating closest RHO expression level, as we observed after siRNA-mediated knockdown in some cell lines used in this study (Figures S5A, S5B, S6H, and S6I). Many proteins display multiple intracellular functions that cannot be individually addressed using genetic approaches, especially when they show different post-translational modifications, conformations, or activity states. Therefore, nanobody or single-domain antibody-mediated protein interference offers a unique approach to monitor selectively their activities at the protein level.

Figure 6. Functional Inhibition of RHOB Activity Accumulated γH2AX Foci

PC9 cells were transfected with smart pool siRNA against RHOB (siRHOB) or control siRNA (siCtl), and with F-NR or F-B6 expression vector for 24 h. Immunofluorescence staining of γH2AX and Myc tag for F-IB-expressing cells were quantified with high-content automated fluorescence microscopy. Nuclei were stained with Hoechst and are surrounded with dash lines in the green channel showing γH2AX foci. Scale bars, 20 μm.

(A) Representative fields of PC9 cell transfected with siRNA. Quantification of foci number per cell using high-content microscopy (see the STAR Methods) is shown as a violin plot from two independent experiments. Mean ± SEM of siCtl is 2.648 ± 0.022 (n = 19,180 cells) and of siRHOB is 3.766 ± 0.025 (n = 17,642 cells).

(B) Western blot showing representative siRNA extinction of RHOB.

(C) Representative fields of PC9 cells transfected with F-Ib IRES Mito-mCherry-expressing plasmid. F-Ib-expressing cells were revealed with Myc tag immunofluorescence. Quantification of foci number per cell from two independent experiments using high-content microscopy (n > 2,000; see the STAR Methods) is shown as a violin plot. Mean ± SEM of F-NR is 4.078 ± 0.057 (n = 3,566 cells) and of F-B6 is 4.916 ± 0.064 (n = 3,645 cells). For each violin plot, the median is shown as a horizontal black line and the 25th and 75th quartiles as dotted black lines.

(D) Western blot showing RHOB-GTP knockdown mediated by F-B6 in PC9 cells. Quantification of RHOB-GTP over total RHOB in F-Ib-transfected cells condition normalized to F-NR is shown as mean ± SD (n = 3 biological repeats). ***p < 0.001.

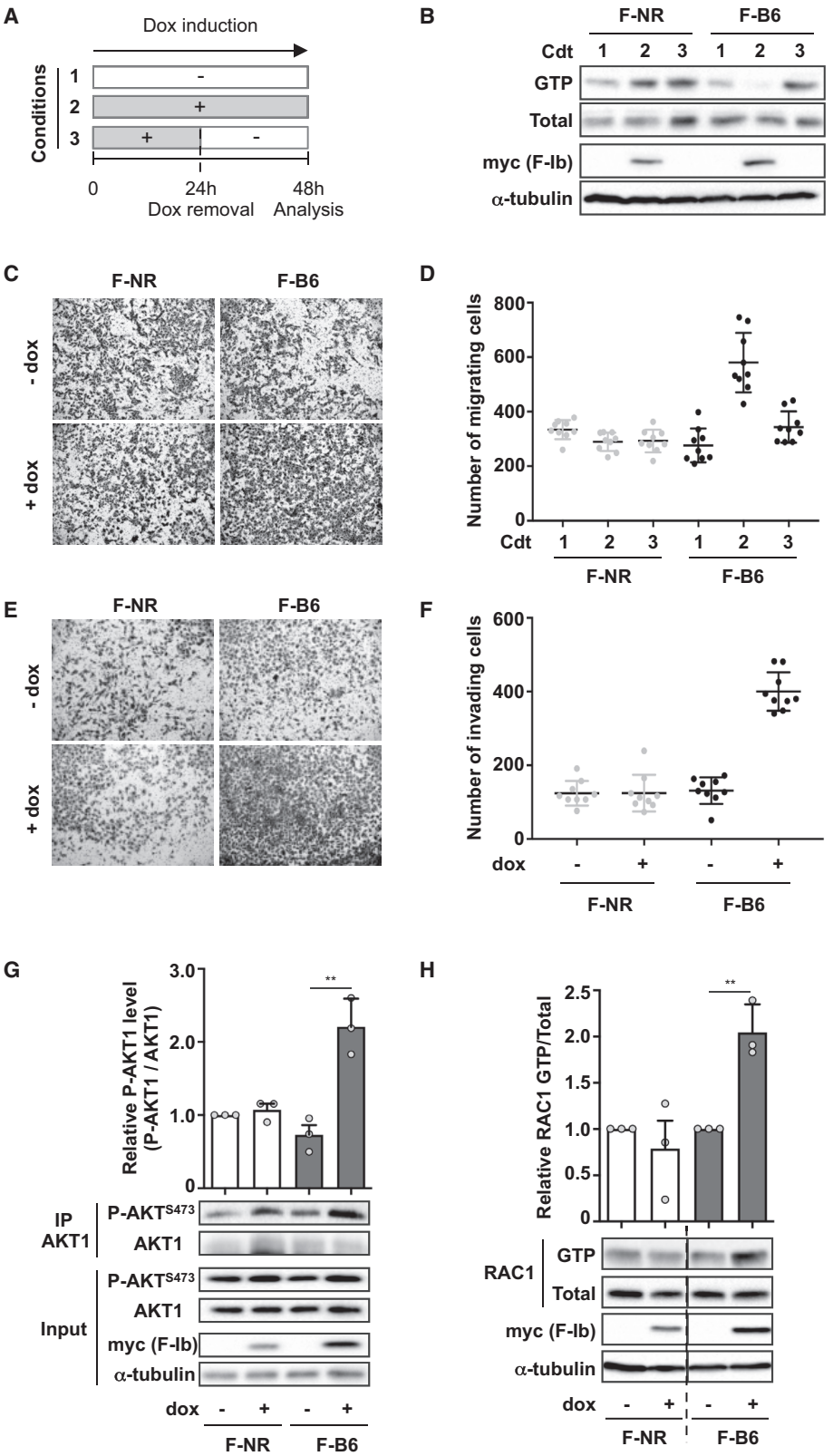

Figure 7. RHOB Activity Knockdown Increases Migration and Invasion of BEAS-2B Cells

(A) Scheme of migration experiment. Cells were not induced (condition 1), induced for 48 h (2) or induced for 24 h, and then doxycycline (dox) was removed for 24 h (3).

(legend continued on next page)

In summary, we present an approach to analyze the role of endogenous RHOB-GTP protein. This strategy is complementary to RHOB-GTP biosensors, which reflect activities of ectopically expressed constructs with either FRET (Reinhard et al., 2016), BRET (Keller et al., 2019) or with the protein complementation assay referred to as tripartite split-GFP (Koraïchi et al., 2017). Targeted protein degradation may be applied to decipher the cellular functions of small GTPases conformational states, and more generally to other cellular targets whose functions are driven by different conformations.

SIGNIFICANCE

The RAS-related RHO-GTPases (RHOA/B/C) switch between a GDP-bound and a GTP-bound state that drives downstream signaling. Studies addressing their function by targeting at the RNA or DNA level to downregulate expression levels of both GDP and GTP fractions indicated an upregulation of closely related RHO as a sign of cellular compensation mechanisms. To formally decipher the role of a single RHO in its GTP conformation, complementary techniques such as targeted protein degradation approaches are particularly suited for degrading selectively post-translationally modified proteins as well as a single conformation of molecular switches. In this study, we engineered a tool based on an F-box-fused single-domain intracellular antibody (F-Ib) to selectively degrade the GTP-bound form of endogenous RHOB. Starting from a subtractive phage display selection of nanobodies, we established a cell-based screen with a visual fluorescent readout of RHOB protein degradation. We identified one intrabody that shows selective targeting of endogenous RHOB-GTP-mediated by interactions between the intrabody CDR3 loop and the GTP-binding pocket of RHOB. In addition, we demonstrated that only the minor GTP-bound fraction, but not its global expression, mediates RHOB functions in genomic instability and in cell invasion. The F-box/intrabody-mediated protein degradation represents a unique approach to selectively target the active form of small GTPases or other proteins with multiple cellular activities.

STAR★METHODS

Detailed methods are provided in the online version of this paper and include the following:

SUPPLEMENTAL INFORMATION

Supplemental Information can be found online at https://doi.org/10.1016/j.chembiol.2019.08.009.

ACKNOWLEDGMENTS

We thank E. Bousquet, O. Calvayrac, and A. Cristini for experimental advice and discussions; and S. Leocadie for comments on the manuscript. The equipment used for crystallization experiments and X-ray crystallography are part of the Integrated Screening Platform of Toulouse (PICT, IBiSA). We acknowledge the Toulouse Genotoul TRI facilities (LBCMCP/CBI) for Operetta high-throughput acquisition and analysis. We thank the European Synchrotron Radiation Facility (ESRF), Grenoble, France, in particular the staff of beamlines ID30A-1. We thank the Pôle Technologique du CRCT—Plateaux Imagerie, Cytométrie and Vectorologie INSERM-UMR1037 for assistance, and L. Ligat for SPR measurements. This work is supported by the cancéropole grand sud ouest (GSO emergence 2014) and the by the grant Fondation pour la Recherche Médicale (FRM) (Equipe labellisée FRM [DEQ20170839117]). N.B. was supported by the Fondation pour la Recherche Médicale (FRM, FDT20130928310).

AUTHOR CONTRIBUTIONS

Conceptualization: N.B., G.F., and A.O.; Methodology: N.B., L.K., A.O., G.F., O.S., I.L.-M., and J.-D.P.; Investigation: N.B., L.K., A.-L.I., M.S., R.G., and J.C.; Writing: N.B., L.K., I.L.-M., S.C., O.S., J.-D.P., G.F., and A.O.; Funding

(B) RHOB-GTP level in BEAS-2B cells is revealed with a GST-RBD pull-down. RHOB-GTP is knocked down when F-B6 expression is induced for 48 h and RHOB-GTP level is restored when dox induction of F-B6 is stopped for 24 h.

(C and D) F-B6 induces BEAS-2B cell migration in a Transwell system compared with the F-NR control and the non-induced condition. Migration is stopped when dox is removed for 24 h (F-B6 condition 3) showing that RHOB-GTP knockdown is directly responsible for cell migration.

(E–H) F-B6 induction increases invasion in Matrigel compared with the non-induced (F-B6–) and the negative control (F-NR) (E and F). Mean ± SD is displayed in (D) and (F), the dots representing the number of cells counted for each repeat (three technical repeats per biological repeat, three biological repeats). These effects are dependent of AKT1 phosphorylation (G) and RAC1 activation (H). AKT1 was immuno-precipitated and revealed with an anti-phospho-S473 AKT antibody. Quantification of three independent immuno-precipitation experiments shows the level of phosphorylated AKT1 normalized to AKT1 level on beads (G). The RAC1-active fraction was revealed with a GST-PAKBD pull-down and three independent experiments were quantified. Relative RAC1 activity was calculated as the ratio between GTP and input levels normalized to each F-Ib non-induced activity (H). Data in (H and G) are normalized means ± SEM (n = 3 biological repeats). $^{**}p < 0.01$. See also Figure S6.

Acquisition: A.O., J.-D.P., S.C., I.L.-M., and G.F.; Supervision: O.S., J.-D.P., I.L.-M., G.F., and A.O.

DECLARATION OF INTERESTS

N.B., L.K., G.F., and A.O. are co-inventors on the patent PTC/EP2016/052136, concerning the discovery of RHO-GTP single-domain antibodies and their applications. The other authors declare no conflict of interest.

Received: May 5, 2018
Revised: November 22, 2018
Accepted: August 23, 2019
Published: September 12, 2019

REFERENCES

Adams, P.D., Afonine, P.V., Bunkóczi, G., Chen, V.B., Davis, I.W., Echols, N., Headd, J.J., Hung, L.-W., Kapral, G.J., Grosse-Kunstleve, R.W., et al. (2010). PHENIX: a comprehensive Python-based system for macromolecular structure solution. Acta Crystallogr. D Biol. Crystallogr. *66*, 213–221.

Adnane, J., Muro-Cacho, C., Mathews, L., Sebti, S.M., and Munoz-Antonia, T. (2002). Suppression of rho B expression in invasive carcinoma from head and neck cancer patients. Clin. Cancer Res. *8*, 2225–2232.

Aktories, K., Mohr, C., and Koch, G. (1992). *Clostridium botulinum* C3 ADP-ribosyltransferase. Curr. Top. Microbiol. Immunol. *175*, 115–131.

Alfano, D., Ragno, P., Stoppelli, M.P., and Ridley, A.J. (2012). RhoB regulates uPAR signalling. J. Cell Sci. *125*, 2369–2380.

Baker, N.A., Sept, D., Joseph, S., Holst, M.J., and McCammon, J.A. (2001). Electrostatics of nanosystems: application to microtubules and the ribosome. Proc. Natl. Acad. Sci. U S A *98*, 10037–10041.

Baron, R., Fourcade, E., Lajoie-Mazenc, I., Allal, C., Couderc, B., Barbaras, R., Favre, G., Faye, J.C., and Pradines, A. (2000). RhoB prenylation is driven by the three carboxyl-terminal amino acids of the protein: evidenced in vivo by an anti-farnesyl cysteine antibody. Proc. Natl. Acad. Sci. U S A *97*, 11626–11631.

Bondeson, D.P., Smith, B.E., Burslem, G.M., Buhimschi, A.D., Hines, J., Jaime-Figueroa, S., Wang, J., Hamman, B.D., Ishchenko, A., and Crews, C.M. (2018). Lessons in PROTAC design from selective degradation with a promiscuous warhead. Cell Chem. Biol. *25*, 78–87.e5.

Bousquet, E., Mazières, J., Privat, M., Rizzati, V., Casanova, A., Ledoux, A., Mery, E., Couderc, B., Favre, G., and Pradines, A. (2009). Loss of RhoB expression promotes migration and invasion of human bronchial cells via activation of AKT1. Cancer Res. *69*, 6092–6099.

Bousquet, E., Calvayrac, O., Mazières, J., Lajoie-Mazenc, I., Boubekeur, N., Favre, G., and Pradines, A. (2015). RhoB loss induces Rac1-dependent mesenchymal cell invasion in lung cells through PP2A inhibition. Oncogene *35*, 1760–1769.

Bustelo, X.R., Sauzeau, V., and Berenjeno, I.M. (2007). GTP-binding proteins of the Rho/Rac family: regulation, effectors and functions in vivo. Bioessays *29*, 356–370.

Calvayrac, O., Mazières, J., Figarol, S., Marty-Detraves, C., Raymond-Letron, I., Bousquet, E., Farella, M., Clermont-Taranchon, E., Milia, J., Rouquette, I., et al. (2017). The RAS-related GTPase RHOB confers resistance to EGFR-tyrosine kinase inhibitors in non-small-cell lung cancer via an AKT-dependent mechanism. EMBO Mol. Med. *9*, 238–250.

Canguilhem, B., Pradines, A., Baudouin, C., Boby, C., Lajoie-Mazenc, I., Charveron, M., and Favre, G. (2005). RhoB protects human keratinocytes from UVB-induced apoptosis through epidermal growth factor receptor signaling. J. Biol. Chem. *280*, 43257–43263.

Caussinus, E., Kanca, O., and Affolter, M. (2011). Fluorescent fusion protein knockout mediated by anti-GFP nanobody. Nat. Struct. Mol. Biol. *19*, 117–121.

Chinestra, P., Lajoie-Mazenc, I., Faye, J.C., and Favre, G. (2012). Use of phage display for the identification of molecular sensors specific for activated Rho. Methods Mol. Biol. *827*, 283–303.

Chinestra, P., Olichon, A., Medale-Giamarchi, C., Lajoie-Mazenc, I., Gence, R., Inard, C., Ligat, L., Faye, J.C., and Favre, G. (2014). Generation of a single chain antibody variable fragment (scFv) to sense selectively RhoB activation. PLoS One *9*, e111034.

Clift, D., McEwan, W.A., Labzin, L.I., Konieczny, V., Mogessie, B., James, L.C., and Schuh, M. (2017). A method for the acute and rapid degradation of endogenous proteins. Cell *17*, 1692–1706.e18.

Connolly, E.C., Van Doorslaer, K., Rogler, L.E., and Rogler, C.E. (2010). Overexpression of miR-21 promotes an in vitro metastatic phenotype by targeting the tumor suppressor RHOB. Mol. Cancer Res. *8*, 691–700.

Couderc, B., Pradines, A., Rafii, A., Golzio, M., Deviers, A., Allal, C., Berg, D., Penary, M., Teissie, J., and Favre, G. (2008). In vivo restoration of RhoB expression leads to ovarian tumor regression. Cancer Gene Ther. *15*, 456–464.

Delmas, A., Cherier, J., Pohorecka, M., Medale-Giamarchi, C., Meyer, N., Casanova, A., Sordet, O., Lamant, L., Savina, A., Pradines, A., et al. (2015). The c-Jun/RHOB/AKT pathway confers resistance of BRAF-mutant melanoma cells to MAPK inhibitors. Oncotarget *6*, 15250–15264.

Emsley, P., Lohkamp, B., Scott, W.G., and Cowtan, K. (2010). Features and development of Coot. Acta Crystallogr. D Biol. Crystallogr. *66*, 486–501.

Etienne-Manneville, S., and Hall, A. (2002). Rho GTPases in cell biology. Nature *420*, 629–635.

Farnsworth, C.L., and Feig, L.A. (1991). Dominant inhibitory mutations in the Mg(2+)-binding site of RasH prevent its activation by GTP. Mol. Cell. Biol. *11*, 4822–4829.

Fritz, G., Kaina, B., and Aktories, K. (1995). The ras-related small GTP-binding protein RhoB is immediate-early inducible by DNA damaging treatments. J. Biol. Chem. *270*, 25172–25177.

Gampel, A., Parker, P.J., and Mellor, H. (1999). Regulation of epidermal growth factor receptor traffic by the small GTPase rhoB. Curr. Biol. *9*, 955–958.

García-Mariscal, A., Li, H., Pedersen, E., Peyrollier, K., Ryan, K.M., Stanley, A., Quondamatteo, F., and Brakebusch, C. (2017). Loss of RhoA promotes skin tumor formation and invasion by upregulation of RhoB. Oncogene *37*, 847–860.

Gerald, D., Adini, I., Shechter, S., Perruzzi, C., Varnau, J., Hopkins, B., Kazerounian, S., Kurschat, P., Blachon, S., Khedkar, S., et al. (2013). RhoB controls coordination of adult angiogenesis and lymphangiogenesis following injury by regulating VEZF1-mediated transcription. Nat. Commun. *4*, 2824.

Goedhart, J., and van Unen, J. (2017). Molecular perturbation strategies to examine spatiotemporal features of Rho GEF and Rho GTPase activity in living cells. Small GTPases *10*, 1–9.

Guglielmi, L., and Martineau, P. (2009). Intrabody expression in eukaryotic cells. Methods Mol. Biol. *562*, 195–203.

Guilluy, C., Dubash, A.D., and García-Mata, R. (2011). Analysis of RhoA and Rho GEF activity in whole cells and the cell nucleus. Nat. Protoc. *6*, 2050–2060.

Haque, A., Andersen, J.N., Salmeen, A., Barford, D., and Tonks, N.K. (2011). Conformation-sensing antibodies stabilize the oxidized form of PTP1B and inhibit its phosphatase activity. Cell *147*, 185–198.

Heasman, S.J., and Ridley, A.J. (2008). Mammalian Rho GTPases: new insights into their functions from in vivo studies. Nat. Rev. Mol. Cell Biol. *9*, 690–701.

Helma, J., Cardoso, M.C., Muyldermans, S., and Leonhardt, H. (2015). Nanobodies and recombinant binders in cell biology. J. Cell Biol. *209*, 633–644.

Ho, T.T.G., Merajver, S.D., Lapière, C.M., Nusgens, B.V., and Deroanne, C.F. (2008). RhoA-GDP regulates RhoB protein stability: potential involvement of RhoGDIα. J. Biol. Chem. *283*, 21588–21598.

Howe, G.A., and Addison, C.L. (2012). RhoB controls endothelial cell morphogenesis in part via negative regulation of RhoA. Vasc. Cell *4*, 1.

Huang, M., and Prendergast, G.C. (2006). RhoB in cancer suppression. Histol. Histopathol. *21*, 213–218.

Joshi, S.N., Butler, D.C., and Messer, A. (2012). Fusion to a highly charged proteasomal retargeting sequence increases soluble cytoplasmic expression and efficacy of diverse anti-synuclein intrabodies. MAbs *4*, 686–693.

Ju, J., and Gilkes, D. (2018). RhoB: team oncogene or team tumor suppressor? Genes *9*, 67.

Kaiser, P.D., Maier, J., Traenkle, B., Emele, F., and Rothbauer, U. (2014). Recent progress in generating intracellular functional antibody fragments to target and trace cellular components in living cells. Biochim. Biophys. Acta *1844*, 1933–1942.

Keller, L., Bery, N., Tardy, C., Ligat, L., Favre, G., Rabbitts, T.H., and Olichon, A. (2019). Selection and characterization of a nanobody biosensor of GTP-bound RHO activities. Antibodies *8*, 8.

Kipreos, E.T., and Pagano, M. (2000). The F-box protein family. Genome Biol. *1*, REVIEWS3002.

Koo, M.Y., Park, J., Lim, J.M., Joo, S.Y., Shin, S.-P., Shim, H.B., Chung, J., Kang, D., Woo, H.A., and Rhee, S.G. (2014). Selective inhibition of the function of tyrosine-phosphorylated STAT3 with a phosphorylation site-specific intrabody. Proc. Natl. Acad. Sci. U S A *111*, 6269–6274.

Koraïchi, F., Gence, R., Bouchenot, C., Grosjean, S., Lajoie-Mazenc, I., Favre, G., and Cabantous, S. (2017). High-content tripartite split-GFP cell-based assays to screen for modulators of small GTPase activation. J. Cell. Sci. *131*, https://doi.org/10.1242/jcs.210419.

Kovačević, I., Sakaue, T., Majoleé, J., Pronk, M.C., Maekawa, M., Geerts, D., Fernandez-Borja, M., Higashiyama, S., and Hordijk, P.L. (2018). The Cullin-3-Rbx1-KCTD10 complex controls endothelial barrier function via K63 ubiquitination of RhoB. J. Cell Biol. *217*, 1015–1032.

Kuo, C.-L., Oyler, G.A., and Shoemaker, C.B. (2011). Accelerated neuronal cell recovery from *Botulinum* neurotoxin intoxication by targeted ubiquitination. PLoS One *6*, e20352.

Lajoie-Mazenc, I., Tovar, D., Penary, M., Lortal, B., Allart, S., Favard, C., Brihoum, M., Pradines, A., and Favre, G. (2008). MAP1A light chain-2 interacts with GTP-RhoB to control epidermal growth factor (EGF)-dependent EGF receptor signaling. J. Biol. Chem. *283*, 4155–4164.

Mamouni, K., Cristini, A., Guirouilh-Barbat, J., Monferran, S., Lemarié, A., Faye, J.-C., Lopez, B.S., Favre, G., and Sordet, O. (2014). RhoB promotes γH2AX dephosphorylation and DNA double-strand break repair. Mol. Cell. Biol. *34*, 3144–3155.

Mandik-Nayak, L., DuHadaway, J.B., Mulgrew, J., Pigott, E., Manley, K., Sedano, S., Prendergast, G.C., and Laury-Kleintop, L.D. (2017). RhoB blockade selectively inhibits autoantibody production in autoimmune models of rheumatoid arthritis and lupus. Dis. Model. Mech. *10*, 1313–1322.

Marcos-Ramiro, B., García-Weber, D., Barroso, S., Feito, J., Ortega, M.C., Cernuda-Morollón, E., Reglero-Real, N., Fernández-Martín, L., Durán, M.C., Alonso, M.A., et al. (2016). RhoB controls endothelial barrier recovery by inhibiting Rac1 trafficking to the cell border. J. Cell Biol. *213*, 385–402.

Mazieres, J., Antonia, T., Daste, G., Muro-Cacho, C., Berchery, D., Tillement, V., Pradines, A., Sebti, S., and Favre, G. (2004). Loss of RhoB expression in human lung cancer progression. Clin. Cancer Res. *10*, 2742–2750.

McCoy, A.J., Grosse-Kunstleve, R.W., Adams, P.D., Winn, M.D., Storoni, L.C., and Read, R.J. (2007). Phaser crystallographic software. J. Appl. Crystallogr. *40*, 658–674.

Melchionna, T., and Cattaneo, A. (2007). A protein silencing switch by ligand-induced proteasome-targeting intrabodies. J. Mol. Biol. *374*, 641–654.

Meyer, N., Peyret-Lacombe, A., Canguilhem, B., Médale-Giamarchi, C., Mamouni, K., Cristini, A., Monferran, S., Lamant, L., Filleron, T., Pradines, A., et al. (2014). RhoB promotes cancer initiation by protecting keratinocytes from UVB-induced apoptosis but limits tumor aggressiveness. J. Invest. Dermatol. *134*, 203–212.

Moutel, S., Bery, N., Bernard, V., Keller, L., Lemesre, E., de Marco, A., Ligat, L., Rain, J.-C., Favre, G., Olichon, A., et al. (2016). NaLi-H1: a universal synthetic library of humanized nanobodies providing highly functional antibodies and intrabodies. Elife *5*, https://doi.org/10.7554/eLife.16228.

Nizak, C., Monier, S., del Nery, E., Moutel, S., Goud, B., and Perez, F. (2003). Recombinant antibodies to the small GTPase Rab6 as conformation sensors. Science *300*, 984–987.

Nowak, R.P., DeAngelo, S.L., Buckley, D., He, Z., Donovan, K.A., An, J., Safaee, N., Jedrychowski, M.P., Ponthier, C.M., Ishoey, M., et al. (2018). Plasticity in binding confers selectivity in ligand-induced protein degradation. Nat. Chem. Biol. *14*, 706–714.

Olson, C.M., Jiang, B., Erb, M.A., Liang, Y., Doctor, Z.M., Zhang, Z., Zhang, T., Kwiatkowski, N., Boukhali, M., Green, J.L., et al. (2017). Pharmacological perturbation of CDK9 using selective CDK9 inhibition or degradation. Nat. Chem. Biol. *14*, 163–170.

Pertz, O., and Hahn, K.M. (2004). Designing biosensors for Rho family proteins—deciphering the dynamics of Rho family GTPase activation in living cells. J. Cell Sci. *117*, 1313–1318.

Pillé, J.-Y., Denoyelle, C., Varet, J., Bertrand, J.-R., Soria, J., Opolon, P., Lu, H., Pritchard, L.-L., Vannier, J.-P., Malvy, C., et al. (2005). Anti-RhoA and anti-RhoC siRNAs inhibit the proliferation and invasiveness of MDA-MB-231 breast cancer cells in vitro and in vivo. Mol. Ther. *11*, 267–274.

Raina, K., and Crews, C.M. (2017). Targeted protein knockdown using small molecule degraders. Curr. Opin. Chem. Biol. *39*, 46–53.

Rakhit, R., Navarro, R., and Wandless, T.J. (2014). Chemical biology strategies for posttranslational control of protein function. Chem. Biol. *21*, 1238–1252.

Reinhard, N.R., van Helden, S.F., Anthony, E.C., Yin, T., Wu, Y.I., Goedhart, J., Gadella, T.W.J., and Hordijk, P.L. (2016). Spatiotemporal analysis of RhoA/B/C activation in primary human endothelial cells. Sci. Rep. *6*, 25502.

Ren, X.D., Kiosses, W.B., and Schwartz, M.A. (1999). Regulation of the small GTP-binding protein Rho by cell adhesion and the cytoskeleton. EMBO J. *18*, 578–585.

Ridley, A.J. (2006). Rho GTPases and actin dynamics in membrane protrusions and vesicle trafficking. Trends Cell Biol. *16*, 522–529.

Sandilands, E., Cans, C., Fincham, V.J., Brunton, V.G., Mellor, H., Prendergast, G.C., Norman, J.C., Superti-Furga, G., and Frame, M.C. (2004). RhoB and actin polymerization coordinate Src activation with endosome-mediated delivery to the membrane. Dev. Cell *7*, 855–869.

Sato, N., Fukui, T., Taniguchi, T., Yokoyama, T., Kondo, M., Nagasaka, T., Goto, Y., Gao, W., Ueda, Y., Yokoi, K., et al. (2007). RhoB is frequently down-regulated in non-small-cell lung cancer and resides in the 2p24 homozygous deletion region of a lung cancer cell line. Int. J. Cancer *120*, 543–551.

Schaefer, A., Reinhard, N.R., and Hordijk, P.L. (2014). Toward understanding RhoGTPase specificity: structure, function and local activation. Small GTPases *5*, 6.

Sebestyen, Z., Scheper, W., Vyborova, A., Gu, S., Rychnavska, Z., Schiffler, M., Cleven, A., Chéneau, C., van Noorden, M., Peigné, C.-M., et al. (2016). RhoB mediates phosphoantigen recognition by Vγ9Vδ2 T cell receptor. Cell Rep. *15*, 1973–1985.

Shang, X., Marchioni, F., Sipes, N., Evelyn, C.R., Jerabek-Willemsen, M., Duhr, S., Seibel, W., Wortman, M., and Zheng, Y. (2012). Rational design of small molecule inhibitors targeting RhoA subfamily Rho GTPases. Chem. Biol. *19*, 699–710.

Shang, X., Marchioni, F., Evelyn, C.R., Sipes, N., Zhou, X., Seibel, W., Wortman, M., and Zheng, Y. (2013). Small-molecule inhibitors targeting G-protein-coupled Rho guanine nucleotide exchange factors. Proc. Natl. Acad. Sci. U S A *110*, 3155–3160.

Sheffield, P., Garrard, S., and Derewenda, Z. (1999). Overcoming expression and purification problems of RhoGDI using a family of "parallel" expression vectors. Protein Expr. Purif. *15*, 34–39.

Skaar, J.R., Pagan, J.K., and Pagano, M. (2013). Mechanisms and function of substrate recruitment by F-box proteins. Nat. Rev. Mol. Cell Biol. *14*, 369–381.

Stultiens, A., Ho, T.T.G., Nusgens, B.V., Colige, A.C., and Deroanne, C.F. (2012). Rho proteins crosstalk via RhoGDIalpha: at random or hierarchically ordered? Commun. Integr. Biol. *5*, 99–101.

Subauste, M.C., Von Herrath, M., Benard, V., Chamberlain, C.E., Chuang, T.H., Chu, K., Bokoch, G.M., and Hahn, K.M. (2000). Rho family proteins modulate rapid apoptosis induced by cytotoxic T lymphocytes and Fas. J. Biol. Chem. *275*, 9725–9733.

Tanaka, T., Williams, R.L., and Rabbitts, T.H. (2007). Tumour prevention by a single antibody domain targeting the interaction of signal transduction proteins with RAS. EMBO J. *26*, 3250–3259.

Tang, J.C., Drokhlyansky, E., Etemad, B., Rudolph, S., Guo, B., Wang, S., Ellis, E.G., Li, J.Z., and Cepko, C.L. (2016). Detection and manipulation of live

antigen-expressing cells using conditionally stable nanobodies. Elife *5*, https://doi.org/10.7554/eLife.15312.

Vega, F.M., and Ridley, A.J. (2008). Rho GTPases in cancer cell biology. FEBS Lett. *582*, 2093–2101.

Vega, F.M., and Ridley, A.J. (2018). The RhoB small GTPase in physiology and disease. Small GTPases *9*, 384–393.

Vega, F.M., Fruhwirth, G., Ng, T., and Ridley, A.J. (2011). RhoA and RhoC have distinct roles in migration and invasion by acting through different targets. J. Cell Biol. *193*, 655–665.

Vega, F.M., Colomba, A., Reymond, N., Thomas, M., and Ridley, A.J. (2012). RhoB regulates cell migration through altered focal adhesion dynamics. Open Biol. *2*, 120076.

Vega, F.M., Thomas, M., Reymond, N., and Ridley, A.J. (2015). The Rho GTPase RhoB regulates cadherin expression and epithelial cell-cell interaction. Cell Commun. Signal. *13*, 6.

Wang, M., Guo, L., Wu, Q., Zeng, T., Lin, Q., Qiao, Y., Wang, Q., Liu, M., Zhang, X., Ren, L., et al. (2014). ATR/Chk1/Smurf1 pathway determines cell fate after DNA damage by controlling RhoB abundance. Nat. Commun. *5*, 4901.

Wennerberg, K., and Der, C.J. (2004). Rho-family GTPases: it's not only Rac and Rho (and I like it). J. Cell Sci. *117*, 1301–1312.

Yoneda, M., Hirokawa, Y.S., Ohashi, A., Uchida, K., Kami, D., Watanabe, M., Yokoi, T., Shiraishi, T., and Wakusawa, S. (2010). RhoB enhances migration and MMP1 expression of prostate cancer DU145. Exp. Mol. Pathol. *88*, 90–95.

Zandvakili, I., Lin, Y., Morris, J.C., and Zheng, Y. (2017). Rho GTPases: anti- or pro-neoplastic targets? Oncogene *36*, 3213–3222.

Zhang, K., and Cui, B. (2015). Optogenetic control of intracellular signaling pathways. Trends Biotechnol. *33*, 92–100.

Zhou, J., Zhu, Y., Zhang, G., Liu, N., Sun, L., Liu, M., Qiu, M., Luo, D., Tang, Q., Liao, Z., et al. (2011). A distinct role of RhoB in gastric cancer suppression. Int. J. Cancer *128*, 1057–1068.

STAR★METHODS

KEY RESOURCES TABLE

REAGENT or RESOURCE	SOURCE	IDENTIFIER
Antibodies		
RHOA Mouse antibody	Santa Cruz Biotechnology	Cat#sc-418; RRID: AB_628218
RHOB Rabbit antibody	Santa Cruz Biotechnology	Cat#sc-180; RRID: AB_2179110
RHOC Rabbit antibody	Cell Signaling Technology	Cat#3430S; RRID: AB_2179246
Phospho-AKT S473 Rabbit antibody	Cell Signaling Technology	Cat#4058S; RRID: AB_331168
Total AKT1 Mouse antibody	Cell Signaling Technology	Cat#2967S; RRID: AB_331160
RAC1 Rabbit antibody	Millipore	Cat# 07-1464; RRID: AB_1977451
α-tubulin Mouse antibody	Sigma-Aldrich	Cat#T9026; RRID: AB_477593
CMYC HRP-linked Goat antibody	Novus Biologicals	Cat#NB600-341; RRID: AB_10000717
GAPDH (D4C6R) Mouse mAb	Cell Signaling Technology	Cat#97166; RRID: AB_2756824
γ-H2AX Mouse antibody	Cell Signaling Technology	Cat#9718S; RRID: AB_2118009
Bacterial and Virus Strains		
E.coli BL21 (DE3) cells	New England Biolabs	Cat#C2527I
E.coli XL1-Blue cells	Stratagene	Cat#200236
Chemicals, Peptides, and Recombinant Proteins		
$RHOB^{Q63L}$	This study	N/A
B6 VHH	This study	N/A
GST-RBD	This study	N/A
GST-PAKBD	This study	N/A
Recombinant Human Epidermal Growth Factor (EGF)	Sigma	Cat#E9644
Protease Inhibitor Cocktail	Sigma-Aldrich	Cat#P8340
Halt™ Phosphatase Inhibitor Cocktail	Thermo-Fisher	Cat#1862495
Zeocin	Invitrogen	Cat#R25001
Bortezomib	Selleckchem	Cat#PS-341
MG-132	Sigma	Cat#C2211
Critical Commercial Assays		
jetPRIME	Polyplus Transfection	Cat#114-15
CellTiter 96® AQueous One Solution Cell Proliferation Assay (MTS)	Promega	Cat#G3582
Deposited Data		
RHOB-GDP structure	Structural Genomics Consortium (SGC)	PDB: 2FV8
$RHOB^{Q63L}$-GTP structure	This study	PDB: 6HXU
$RHOB^{Q63L}$-GTP/B6 VHH structure	This study	PDB: 6SGE
Experimental Models: Cell Lines		
Human: HEK293 cells	ATCC	Cat#CR-1573
Human: HeLa S3 cells	ATCC	Cat#CCL-2.2
Human: PC9 cells	ECACC	Cat#90071810
Human: NCI-H2882 cells	Sato et al., 2007	RRID:CVCL_5158
Human: BEAS-2B cells	ATCC	Cat#CRL-9609
Recombinant DNA		
p-F-Ib-6xHis-myc-IRES-Mito-mGFP	This study	N/A
p-Ib-mGFP	This study	N/A
p-Ib-6xHis-myc-IRES-Mito-mGFP	This study	N/A
p-H2B-mCherry-RHOBQ63LdeltaCAAX-IRES-Zeo	This study	N/A

(*Continued on next page*)

Continued

REAGENT or RESOURCE	SOURCE	IDENTIFIER
p-H2B-mCherry-RHOB N19deltaCAAX-IRES-Zeo	This study	N/A
p-H2B-mCherry-RAC1 L61deltaCAAX-IRES-Zeo	This study	N/A
p-H2B-mCherry-IRES-Zeo	This study	N/A
p-F-Ib-IRES-BFP	This study	N/A
pTRIP-TRE-MCS XNCA	A gift from Loic Van Den Berghe	N/A
pET-His-TEV-RHOBΔ11Q63L	This study	N/A
pHEN-B6-CBD-2Strep-6xHis	This study	N/A
Software and Algorithms		
Prism 6.0 and 8.0	GraphPad	https://www.graphpad.com/scientific-software/prism/
Phenix	Adams et al., 2010	https://www.phenix-online.org/
PyMOL	Schrodinger	https://pymol.org/2/
Columbus Image Analysis System	PerkinElmer	http://www.perkinelmer.com/product/image-data-storage-and-analysis-system-columbus
Harmony High Content Imaging and Analysis Software	PerkinElmer	http://www.perkinelmer.com/product/harmony-4-8-office-hh17000001
Other		
HiLoad Superdex 75 16/60 column	GE Healthcare	Cat#28989333

LEAD CONTACT AND MATERIALS AVAILABILITY

Further information and requests for resources and reagents should be directed to and will be fulfilled by the Lead Contact; Aurelien Olichon email: aurelien.olichon@inserm.fr.

EXPERIMENTAL MODEL AND SUBJECT DETAILS

Cell Culture, Transient Transfection and Treatment

HeLa S3 cell lines (Cervical adenocarcinoma; ATCC, CCL-2.2 obtained from Yvan Martineau, CRCT), Human bronchial epithelial cell lines BEAS-2B (ATCC CRL-9609), PC9 cells (Lung adenocarcinoma, PC-9 (formerly known as PC-14) (ECACC 90071810) and HEK293 (ATCC CR-1573) were grown in DMEM supplemented with 10% FCS and H2882 stable cell lines were grown in RPMI supplemented with 10% FCS at 37°C in a humidified incubator with 5% CO_2.

METHOD DETAILS

Cell Transfection and Treatment

Transient transfection of small interfering RNA (siRNA; Eurogentec) and DNA plasmids were performed using the Jet Prime method, as indicated by the supplier (PolyPlus Transfection) or RNAimax (Thermofisher). RNAi was performed with a smartpool siRNA kit specific of RHOB and its respective scrumble control siRNA (Dharmacon).

Epithelial Growth Factor (EGF, Sigma) treatment was performed at 50 $ng.mL^{-1}$ after 24h of serum deprivation. Proteasome inhibition was done adding 1 μM of proteasome inhibitor MG132 (Sigma) or 1 μM bortezomib (Selleckchem) in cell growth medium for 36h. Induction of F-Ib expression in BEAS-2B stable cells lines was done using doxycycline (Clontech).

Stable Cell Lines Establishment

40,000 cells / well in a 24 wells plate were plated. The day after, cells were transfected with JetPrime: 0.75 μg of plasmidic DNA + 1.5 μL of JetPrime in 50 μL of JetPrime buffer. 4h after, the transfection was stopped. 72h after transfection, cells were trypsinized and diluted at these concentrations: 1/50, 1/150 or undiluted and then each dilution was plated on a culture dish (100 mm) with 100 $\mu g.mL^{-1}$ of Zeocin (Invitrogen). Every 4 days the medium was changed with new Zeocin. After 3 or 4 weeks, clones appeared and were trypsinised and plated on a 96 wells plate. Antibiotic was always maintained in the culture medium (50 $\mu g.mL^{-1}$).

Production of stable cell lines with tetracycline inducible (Tet-on) F-Ib expression: each p-F-Ib-IRES-BFP lentivirus was produced according to the tri-transfection procedure using the plasmids pLvPack and pLvVSVg (Sigma) in HEK 293T cells for viral production. BEAS-2B cells were previously transduced with the rtTA doxycycline-inducible transactivator, and then cells were further transduced with the F-IB-IRES-BFP lentivirus containing supernatant.

Molecular Cloning

p-F-Ib-IRES-Mito-mGFP and p-Ib-IRES-Mito-mGFP construction: vectors expressing no-Fbox or amino terminal Fbox-fused Ib-6His-Myc as a first cistron followed by IRES-MTS-FP as a second cistron. A PCR was performed to extract the F-box sequence from the following plasmid: NSlmb-VHHGFP4 using BspHIF-boxFw (5' GTTCATGTCATGATGAAAAT GGAGACTG ACAAAATAATGG 3') and F-boxNcoRev (5' CAAGATCCCATGGCGAGGTGGCGGCCAGTC CGCCAGTTG 3') primers. This fragment was inserted in the p-Ib plasmid (intrabodies expression vector with CMV promotor) by digesting with BspHI and NcoI. Then IRES-MTS-fluorescent protein was inserted by PCR downstream of the VHH. EMCV IRES was amplified from pIRES vector with insertion of flanking downstream restriction sites AgeI, NheI and Acc65I. Then a mitochondrial targeting sequence (MTS) from subunit VIII of human cytochrome c oxidase (pEYFP-MTS, Clontech) was inserted between NheI / AgeI, followed by them mGFP between AgeI / Acc65I, thus creating the p-F-Ib_IRES_Mito-GFP in which any Ib can be inserted by NcoI and NotI cloning sites.

p-H2B-mCherry-RHOBQ63LdeltaCAAX-IRES-Zeo construction: a first PCR using pcDNA3.1 Hygro H2B was performed in order to extract H2B sequence with the NotIH2BFw (5' ATTCTTAGCGGCCGCGCCACCATGCCAGAGCCAGCGAAG TCTGCTCCCG 3') and the H2BAgeIRev (5' GACCGGTGAACCGCCACC GCTGCCACCGCCATCCTTAGCGCTGGTGT ACTTGG 3') primers. Then another PCR was performed to extract mCherry sequence from the pAOint4VHH-mCherry plasmid: AgeImCherryFw (5' GCAG CGGTGGCGGTT CACCGGTGGGTATGGTGAGCAAGGGCGAGGAGG 3') and mCherryBsrGIlinkAcc65IRev (5'GCGGAAGGATCC GACCACCTATTAGGTACCGCCTGCGCTACCGCCTGTACACTTGTACAGCTCGTCCATGCCGCC 3'). Then PCR1 + PCR2 were linked with the NotIH2BFor and CherryBsrGIlinkAcc65IRev primers to obtain H2B-mCherry.

Then we extracted the IRES-Zeo sequence from the pIRESZeo-RHOB plasmid (Baron et al., 2000) with the following primers: IRESFw (5' GCAGGCGGTACCTAATAGGT GGTCGGATCCTTCCGCCCCTCTCCCTCCCCCC 3') and ZeoPmeI2BglIIRev (5' TACT AAGAGATCTGTTTAAACTATTAGTCCTGCTCCTCGGCCACGAAGTGCACGCAG 3'). Finally, H2B-mCherry and IRESZeo were linked with the NotIH2BFor and ZeoPmeI2BglIIRev primers and inserted into the pIRES-Zeo-RHOB vector digested with NotI/BamHI. We obtained the p-H2B-mCherry-IRES-Zeo plasmid. We next inserted the active mutants of RHOB (RHOB L63) and RAC1 (RAC1 L63) and the inactive mutant of RHOB (RHOB N19) by digesting the pH2B-mCherry-IRES-Zeo vector by KpnI/BamHI allowing the formation of the following plasmids: p-H2B-mCherry-RHOB L63deltaCAAX-IRES-Zeo; p-H2B-mCherry-RHOB N19deltaCAAX-IRES-Zeo; p-H2B-mCherry-RAC1 L61deltaCAAX-IRES-Zeo.

p-F-Ib-IRES-BFP lentiviral construction: F-Ib-IRES was inserted in the pTRIP-TRE-MCS XNCA lentiviral plasmid (gift from Loic Van Den Berghe) by XbaI / AgeI digestion of the p-F-Ib-IRES-Mito-mGFP plasmid and TagBFP, amplified from pTagBFP-actin plasmid (Evrogen) with the following primers : AgeIBFPFw (5' TTATGCACCGGTGGGTATGAGCGAGCTGATTAAGG 3') and ClaIBFPRev (5' AAGATCTGTACATCGATTAC TAATTAAGCT TGTGCCCCAG TTTGC 3'), was inserted after AgeI / ClaI digestion, thus creating p-F-Ib-IRES-BFP lentiviral vector.

Cloning of RHOB and B6 for X-ray studies. RHOBΔ11Q63L was amplified by PCR using forward 5'-(GGAATTGTGAGCGGATAA CAATTCCC)-3' and reverse 5'-(TGTCGTGAATTCTTATCAGGAGCCGTAGCGCTTCTGCAG)-3' primers. Gel extracted and cleaned inserts from EcoRI/KpnI restriction digests were ligated into the expression vector pHisparallel2 (Sheffield et al., 1999) and transformed into chemically competent BL21 (DE3) star cells (Thermofisher). This vector allows expressing the protein of interest with an N-terminal His tagged followed by a linker sensitive to the tobacco etch virus (TEV) protease. The sequence encoding active mutants of RHOB (RHOB L63), RHOA (RHOA L63) and RHOC (RHOC L63) were cloned KpnI/EcoRI into the same vector. The mutant R133K of RHOB was created by inverted PCR using the QuikChange Site-Directed Mutagenesis Kit (Agilent) using forward 5'-(CGCACAGAGCTGGCCAAGATGAAGCAGGAACCCGTG)-3' and reverse 5'-(CACGGGTTCCTGCTTCATCTTGGCCAGCTCTGT GCG)-3' primers. B6 cDNA was subcloned from the p-F-Ib-IRES-Mito-mGFP vector into the periplasmic expression vector pHEN-CBD-2S-6his digested NcoI/NotI. This vector allows expressing the protein as a fusion of the C terminus of CBD 2S His-tagged. A linker sensitive to the tobacco etch virus protease was added by site-directed mutagenesis using QuickChange Site-Directed Mutagenesis Kit (Agilent) using forward 5'-(TAGCGCGGCCGCTGAAAACCTGTATTTTCAGGGTGGCGGTGGCA)-3' and reverse 5'-(TGCCACCGCCACCCTGAAAATACAGGTTTTCAGCGGCCGCGCTA)-3' primers. Picked clones were grown overnight at 37°C in culture tubes containing 3 mL TB medium supplemented with ampicillin (100 $\mu g.mL^{-1}$) prior to storage in 20% glycerol at -80°C. p-F-Ib-IRES-Mito-mGFP, p-Ib-IRES-Mito-mGFP, p-Ib-GFP, p-H2B-mCherry-RHOB L63deltaCAAX-IRES-Zeo will be available on Addgene.

Subtractive Phage Display Panning for Isolating RHOB-GTP Specific Ib

NaLi-H1 library of humanized synthetic single domain antibody (Moutel et al., 2016) was used for this study. A subtractive panning protocol was designed to isolate antibodies selective for the RHOB-GTP. Chitin binding domain from chitinase A1 (CBD) or twinstrep tag (IBA) fusion of RHOB GTPase active mutant (RHOB L63) were expressed transiently during 24h in HEK293 cells and captured freshly after cell lysis on magnetic beads before incubation with the library phages. Chitin magnetic beads (NEB) or strepTactin coated magStrep HC (IBA) were use. A phage display panning alternating rounds on chitin beads with rounds on streptactin beads was performed during 4 rounds. From the second round of panning, a depletion step on GDP loaded wild type RHOB or N19 inactive mutant was included. Incubate the adequate amount of biotinylated antigen coated beads for 2h with the phage library (10^{13} phages diluted in 1 mL of PBS + 0.1% Tween 20 + 2% non-fat milk). Phages were previously adsorbed on empty streptavidin-coated magnetic beads (to remove nonspecific binders). Recover phage bound to streptavidin-coated beads on a magnet. Wash 10 times (round 1) or 20 times (rounds 2-4) with PBS+Tween 0.1% on a magnet. Elute bound phages using triethylamine (TEA,

100 mM): add 500 μL TEA for 10 min, recover TEA + eluted phages on a magnet and neutralize using 1M Tris pH 7.4. Repeat the elution once more. Infect E. coli (TG1) with the eluted phages. For round 2 to round 4, only 10^{12} phages were used as input.

NaLi-H1 library phages production was mixed in solution with of constitutively active mutant of RHOB (RHOB L63). This mutant was expressed in HEK293 as a carboxy terminal fusion to chitin binding domain from chitinase A1 (CBD-RHOB L63), then freshly pulled-down on chitin magnetic beads for the first round of panning. In subsequent rounds of selection, a tandem repeat of a streptactin binding tag used together with streptactin magnetic beads were alternatively used with the CBD pull-down to avoid tag binding phage. To enrich in GTP-bound RHOB-binding phages, a depletion step was introduced, after the first round of selection, using GDP-bound RHOB proteins before proceeding for the selection against the active RHOB L63. Then from the third round of phage display, a competition step was introduced with RHOA L63 and RHOC L63 mutants to remove non-selective binders. A total of four rounds of panning were performed. The input phages were preincubated with the magnetic beads before each round of panning to eliminate beads binding phage.

Cell-Based Screen

Following 4 rounds of phage display panning, enriched Ibs were subcloned as a polyclonal pool in the p-F-Ib-IRES-Mito-mGFP bicistronic vector. Sequencing a set of 50 individual clones revealed that the F-B20 was over-represented up to 50% of the clones, the other half being fully diverse. Plasmid miniprep of 300 Ib clones were transfected in the visual cell-based protein interference assay in the HmRHOB L63 cell line and analyzes by fluorescent microscopy was performed 48h post transfection on cells fixed 30 minutes in 3.7% PFA. Positive hits were then transfected in both HmRHOB L63 and Hm cell lines to assess the specificity towards RHOB.

Immunofluorescence Staining

Transfected cells were either fixed in 3.7% paraformaldehyde and directly mounted in Mowiol, or permeabilized with PBS-Triton 0.1%, blocked with PBS-BSA 8%, incubated with a mouse monoclonal anti-myc tag (clone 9E10, a gift from S. Moutel) and with an Alexa 488 or 350 secondary antibody (Invitrogen) and mounted in Mowiol. Data acquisition was carried out on a Nikon Eclipse 90i and image processing with NIS Elements v3 software.

Flow Cytometry Analysis

48h after transfection, at least 10,000 cells were analyzed on a MoFlo Astrios flow cytometer for their nuclear mCherry fluorescence intensity. This fluorescence was analyzed in mGFP transfected cells and non-transfected cells. Flow cytometry data were analyzed with Kaluza software (Beckman Coulter).

Western Blot Analyses

Cell extracts were separated on SDS-PAGE and electrotransferred onto polyvinylidene difluoride (PVDF) membranes. Western blots were probed with a rabbit polyclonal anti-RHOB (Santa Cruz Biotechnology®), mouse monoclonal anti-RHOA (Santa Cruz Biotechnology®), mouse monoclonal RHOC (Cell Signaling Technology), rabbit polyclonal anti-phosphorylated AKT (S473, Cell Signaling Technology), mouse monoclonal anti-AKT1 (Cell Signaling Technology), goat polyclonal anti-myc tag HRP conjugated (Novus Biologicals®), mouse monoclonal anti-tubulin (Sigma), rabbit polyclonal anti-RAC1 (Millipore) and mouse monoclonal anti-GAPDH (Cell Signaling Technology®). Detection was performed using peroxydase-conjugated secondary antibodies and chemiluminescence detection kit using the Chemidoc® imaging system (Biorad).

Affinity Measurement

All binding studies based on SPR technology were performed on BIAcore T200 optical biosensor instrument (GE Healthcare). Capture of single domain Hs2dAb-6xHis was performed on a nitrilotriacetic acid (NTA) sensorchip in HBS-P+ buffer (10 mM Hepes pH 7.4, 150 mM NaCl, and 0.05% surfactant P20) (GE Healthcare). The four flow cells (FC) of the sensorchip were used: one (FC 1) to monitor nonspecific binding and to provide background corrections for analyses and the other three flow cells (FC 2, 3, and 4) containing immobilized Hs2dAb-6xHis for measurement.

For immobilization strategies, the four flow cells were loaded with nickel solution (10 $\mu L.min^{-1}$ for 60 s) in order to saturate the NTA surface with Ni^{2+} and an extra wash using running buffer containing 3mM EDTA after the nickel injection. Each His-tagged hs2dAb in running buffer was injected in flow cells at a flow-rate of 10 $\mu L.min^{-1}$. The total amount of immobilized hs2dAb-6xHis was 250-300 resonance units. (RUs; 1 RU corresponds approximately to 1 $pg.mm^{-2}$ of protein on the sensorchip). A Single-Cycle Kinetics (SCK) analysis to determine association (on-rates), dissociation (off-rates) and affinity constants (kon, koff and KD respectively) was carried out. SCK method prevents potential inaccuracy due to sensorchip regeneration between cycles which are necessary in the conventional multiple cycle kinetics (MCK). SCK binding parameters are evaluated for each injection according to the tools and fit models of the BIAevaluation software, giving similar values than MCK. As hs2dAb were smaller proteins than their respective antigens, hs2dAbs were captured on the sensorchip while the recombinant antigens were used as analytes. Purified RHO L63 active or N19 inactive mutants were used as analytes after 6xHis tag removal. Analytes were injected sequentially with increased concentrations ranging between 25 nM to 400 nM in a single cycle without regeneration of the sensorship between injections. Affinities of the RHOB-L63-K133 and RHOB-L63 mutant were measured in parallel at 4°C, due to the poor stability of the K133 mutant. Binding parameters were obtained by fitting the overlaid sensorgrams with the 1:1. Langmuir binding model of the BIAevaluation software version 1.0.

Quantification of RHO and RAC1 Activation

Pull-down of endogenous activated RHO or RAC proteins were performed as previously established. Cells (5.10^6 per pull-down) were lysed in buffer (50 mM TrispH7.4, 500 mM NaCl / 10 mM $MgCl_2$ / 0.5% TritonX100) for GST-RBD pull-down or in buffer (50 mM Tris-HCl, 500 mM NaCl, 1% Triton X-100, 10 mM $MgCl_2$, 2.5 mM EGTA, and 0.5% sodium deoxycholate) for GST-PAKBD pull-down, each buffer supplemented with protease and phosphatase inhibitors. GST-RBD or GST-PAKBD (30 μg) was incubated with cleared lysate for 45 min at 4°C. Beads were washed three times with washing buffer (50 mM Tris-HCl, pH 7.5, 150 mM NaCl, 10 mM $MgCl_2$, 0.1% Tween20) and denatured in 2X Laemmli reducing sample buffer, boiled for 5 min and separated on 12.5% SDS-PAGE for Western Blot analysis.

Immunoprecipitation

For phospho-AKT immunoprecipitation, cells were harvested in cell lysis buffer (50 mM Tris-HCl, 150 mM NaCl, 1% NP-40, 10% glycerol, 1 mM EDTA, 1 mM EGTA, 5 mM $MgCl_2$), supplemented protease and phosphatase inhibitors. Cleared lysate (0.5 mg) was then incubated with 2 μg of antibodies and 50 μL of protein A/G PLUS-Agarose (Repligen) for 4h at 4°C. Beads were washed three times in lysis buffer, and immunoprecipitates were then analyzed by Western blotting.

Pull-down of endogenous RHO proteins loaded in active or inactive state was adapted from well-established GST-RBD pull-down. HeLa cells (5.10^6 per immunoprecipitate) were lysed in buffer (50 mM Tris pH 7.4, 500 mM NaCl, 10 mM $MgCl_2$, 0.5% TritonX100). Crude protein lysates extract was either incubated directly with beads or used for guanine nucleotide loading. For loading, extract was split into 2 and equal volume were loaded with 0.2 mM GTPγS or 2 mM GDP in buffer supplemented with 10 mM EDTA for 30 min at 30°C. Reaction was stopped by adding 30 mM $MgCl_2$. Nanobodies expressed with 6xHis and Myc tags were captured on cOmplete His-Tag Purification Resin (Roche). GST-RBD (40 μg) beads were used as positive control. Beads were incubated with loaded protein suspension for 45 min at 4°C, then washed 3 times with 50 mM Tris-HCl. pH 7.5, 150 mM NaCl. 10 mM $MgCl_2$, 0.1% Tween20 and denatured in 2X Laemmli reducing sample buffer, boiled for 5 minutes and separated on 12.5% SDS-PAGE for Western Blot analysis. Co-precipitations were revealed with anti-RHOB (or anti RHOA or anti RHOC) antibody and Myc antibody followed by HRP-conjugated secondary antibodies.

DNA Damage High Content Microscopy

PC9 cells were plated in 96-well plates, 6,000 cells per well for siRNA transfection with lipofectamine RNAi max (Thermofisher) or 10,000 cells per well for F-IB expression plasmid transfection with Jet Prime kit (Polyplus). The day after, the cells were transfected for 24h. After fixation, permeabilization and saturation steps, γ-H2AX was stained 2 hours with a rabbit anti-γ-H2AX monoclonal antibody (clone 20E3, Cell Signaling Technology) and the secondary antibody anti-mouse Alexa 488 (Molecular Probes). F-Ib expressing cells were detected with anti myc tag mouse monoclonal antibody (clone 9E10) and the secondary antibody Alexa-647 (Molecular Probes). Nuclei were labeled with Hoechst 33342 (Sigma) at a final concentration of 1 $\mu g.mL^{-1}$ for 10 min. Clustering of γ-H2AX foci was further analyzed with an Operetta automated high-content screening microscope (PerkinElmer). For quantitative image analysis, more than 30 fields per well were acquired with a 20× objective lens to visualize approximately 20 000 cells/well using the integrated software Harmony® (PerkinElmer). Each picture was analyzed with the integrated software Columbus (PerkinElmer). Briefly, the Hoechst nuclei were selected according to the B method, and appropriate parameters, such as the size, roundness and intensity of fluorescent objects, were applied to eliminate false positive. In F-Ib treated conditions, Alexa-647 positive cells were detected according to fluorescent intensity and defined as a subpopulation, leading to more than 2,000 counted cells per well. Then the Alexa 488–γ-H2AX foci were detected with the C method with the following parameters: detection sensitivity, 1; splitting coefficient, 1; radius < 5 pixels; background correction, > 0.16. We retained the selection of γ-H2AX focus number according to focus intensity maxima determination. The number of γ-H2AX foci was quantified for two biological replicates in each condition.

Migration and Invasion Assays

The migration and invasion assays were performed as describe elsewhere (Bousquet et al., 2009) with a Transwell system (8-μm pore size, BD Biosciences). Briefly, cells (20.10^3 or 25.10^3 per well) were added in serum-free medium in the upper compartment of the filter. The bottom chamber was filled with complete medium. At 24 or 48h later, cells on the bottom surface of the filter were counted, after staining, under a Nikon inverted microscope in three randomized fields of 505 mm. Cell invasion assay was performed in conditions similar to above, with wells precoated with Matrigel (BD Biosciences). 48 hours later, cells were fixed, stained, and counted as above.

MTS Assay

2,000 cells per well were seeded in 96 well plates. 24h after, cells were induced with different doxycycline's concentrations for 48h (cell viability assay) or induced at 1 $\mu g.mL^{-1}$ for 24, 48 or 72h (proliferation assay). The relative number of viable cells was measured by incubating cells with MTS reagent (CellTiter 96® AQueous One Solution Cell Proliferation Assay from Promega) following the manufacturer's recommendations. Relative cell survival in the presence of doxycycline was normalized to the non-induced cells after background corrections.

Production and Purification of RHOB-GTP and RHOB-GTP/B6

RHOB variants as well as control recombinant RHO proteins with N-terminal His-tag and TEV cleavage site were expressed in BL21 Star (DE3) pRARE *E.coli* cells from a pET vector. Transformed bacteria cell were used to grow 20 mL LB-ampicillin (100 $\mu g.mL^{-1}$) cultures overnight at 37°C prior to inoculation in baffled flasks containing 4 L of the same media. Cells were allowed to grow for approximately 2 h at 37°C before temperature was dropped from 37°C to 20°C. When OD_{600} reached 0.5-0.7, cells were induced with IPTG at a final concentration of 50 μM and grown for an additional 16 h prior to harvesting by centrifugation at 4,000×*g* for 20 min. The pellets were resuspended in buffer A (100 mM Tris HCl pH 8, 150 mM NaCl, 5 mM $MgCl_2$, 5% glycerol, 1 mM TCEP, 10 μM GTPγS) and lysed by sonication on ice prior to centrifugation (1 h, 20,000 g, 4°C). The soluble cell extract was purified by affinity chromatography on a HiTrap Talon crude column (GE Healthcare) equilibrated with buffer A. RHOB was eluted with a linear gradient from 0 to 100% of buffer B (buffer A containing 300 mM imidazole). The peak fractions were pooled and the tag cleavage was performed with AcTev protease (Invitrogen) during dialysis against buffer A (16 h at 4°C). The tag was removed by affinity chromatography using Ni-NTA beads (Clontech). RHOB was further purified by size-exclusion chromatography on a HiLoad Superdex 75 16/60 (GE Healthcare) column equilibrated with buffer B (50 mM Tris HCl pH 8,5, 50 mM NaCl, 5 mM $MgCl_2$, 5% glycerol, 1 mM TCEP, 10 μM GTPγS). RHOB-GTP was concentrated to 9.3 $mg.mL^{-1}$ prior to crystallization trials.

B6 followed by TEV cleavage site and 6xHis was produced in XL1-blue *E.coli* cells (Agilent) in a TB-ampicillin (100 $\mu g.mL^{-1}$) selective medium supplemented with 1% glucose in the start culture and 0.1% glucose after induction with 1 mM IPTG at 28°C for 16 h. The cells were harvested and resuspended in 15 mL ice-cold TES (100 mM Tris pH 8, 1 mM EDTA, 500 mM sucrose) prior to storage at -80°C. 30 mL of a one-quarter dilution of TES buffer was added to the resuspended pellets prior to shaking for 45 min at 4°C. After centrifugation (1h, 20,000g, 4°C), the periplasmic extract containing B6 was incubated 2 h in the presence of His-Tag purification beads (Roche) equilibrated with buffer A. The purification protocol included step gradients of 20, 50 and 400 mM imidazole. The peak fractions were pooled and the tag cleavage was performed with AcTev protease (Invitrogen) during dialysis (16 h, 4°C). The tag was removed by affinity chromatography using Ni-NTA beads (Clontech).

Purification of the RHOB/B6 complex was achieved by incubating the RHOB soluble cell extract with purified B6 for 1 h at 4°C. The complex was purified by affinity chromatography following the same protocol as for B6. RHOB/B6 was further purified by size-exclusion chromatography on a HiLoad Superdex 75 16/60 (GE Healthcare) column equilibrated with buffer B. The complex was concentrated to 13.6 $mg.mL^{-1}$ (OD measurements at 280 nm using an extinction coefficient of 51340 $mol^{-1}.cm^{-1}$) prior to crystallization trials.

Crystallization and Structure Determination

Crystallization trials were set-up at 12°C using commercially available kits from Qiagen (Venlo, Netherlands) in Innovaplate SD-2 (Innovadyne, Australia). The plates were filled using a Nanodrop ExtY crystallization robot (Innovadyne Technologies, Santa Rosa, CA, USA) prior to storage and imaging using a Rock Imager 1000 (Formulatrix, Bedford, MA, USA). Drops containing 200 nL of purified RHOB-GTP or the RHOB-GTP/B6 were mixed with 200 nL of the reservoir solution. Best crystallization conditions for RHOB-GTP were obtained in the presence of 0.1 M MES pH 6, 30% v/w PEG 6000. Diffraction data on RHOB-GTP crystals directly flash frozen in liquid nitrogen were collected to a maximum resolution of 1.19 Å on ID23-1 at the ESRF synchrotron site (Table S1). RHOB-GTP crystals belong to space group $P22_12_1$ with cell parameters a=38.9 Å b=61.5 Å, c=76.7 Å and one molecule per asymmetric unit. Best crystallization conditions for RHOB-GTP/B6 were obtained in the presence of 0.1 M MES pH6.5; 0.2 M $MgCl_2$; 25% v/w PEG4000. Diffraction data were collected to a maximum resolution of 1.5 Å on ID29 at the ESRF synchrotron site. Crystals of the RHOB-GTP/B6 complex belong to space group $P12_11$ with cell parameters a=66.8 Å, b=70.2 Å, c=71.2 Å, β=107.7° and four molecules (2 RHOB and 2 B6) in the asymmetric unit. Both X-ray structures were solved by molecular replacement using the structure of RHOB-GDP (PDB code 2fv8) as a template in PHASER (McCoy et al., 2007). Iterative cycles of manual model building in COOT (Emsley et al., 2010) and refinement procedures using PHENIX refine (Adams et al., 2010) were applied until convergence. Data collection, phasing and refinement statistics are indicated in Table S1.

QUANTIFICATION AND STATISTICAL ANALYSIS

Values reported represent mean ± standard deviation (SD) or standard error of mean (SEM) of at least three independent experiments. Unless indicated otherwise, P values were calculated with GraphPad Prism 6 using a Student's t-test. *, $p<0.05$; **, $p<0.01$; ***, $p<0.001$; ****, $p< 0.0001$.

DATA AND CODE AVAILABILITY

The accession numbers for RHOB-GTP/B6 and RHOB-GTP reported in this paper have been deposited in the Protein Data Bank: codes 6SGE and 6HXU.

Cell Chemical Biology, Volume *26*

Supplemental Information

A Targeted Protein Degradation Cell-Based Screening for Nanobodies Selective toward the Cellular RHOB GTP-Bound Conformation

Nicolas Bery, Laura Keller, Marjorie Soulié, Rémi Gence, Anne-Laure Iscache, Julia Cherier, Stéphanie Cabantous, Olivier Sordet, Isabelle Lajoie-Mazenc, Jean-Denis Pedelacq, Gilles Favre, and Aurélien Olichon

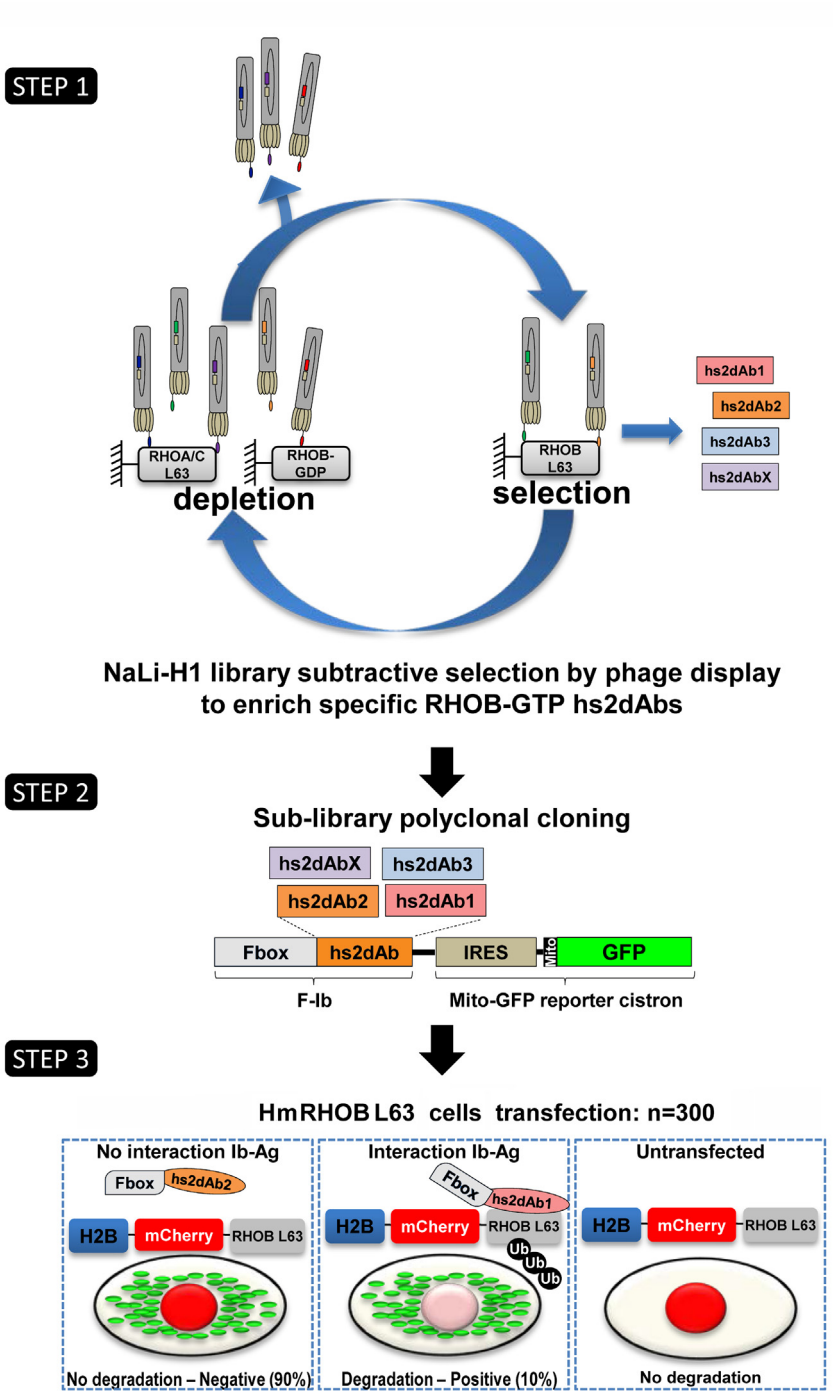

Figure S1: related to Figure 1. Scheme of the direct selection screen of intrabodies degrading active RHOB. Step1: A subtractive phage display to enrich binders of RHOB GTP loaded form was performed on the NaLi-H1 library of humanized synthetic single domain antibodies (hs2dAb). Competition or depletion steps were performed on RHOB-GDP as well as on RHOA/C L63 mutant mimicking GTP-bound state followed by selection on RHOB-GTP. Step2: sub-libraries of the 4th round of phage display hs2dAbs were cloned to be expressed as intrabodies into the p-F-Ib-IRES-Mito-mGFP plasmid, that allows expression of both F-box-Ib-6his-Myc and a Mito-GFP as a fluorescent reporter to visualize transfected cells expressing the prey Ib during the screen. Step3: 300 constructions were then transfected as individual clones into the H2882 cells stably expressing H2B-mCherry-RHOB L63deltaCAAX (HmRHOB L63 cell line). Transfected cells using pF-Ib-IRES-Mito-GFP display green fluorescent mitochondria. Positive hits induce nuclear red fluorescence decay.

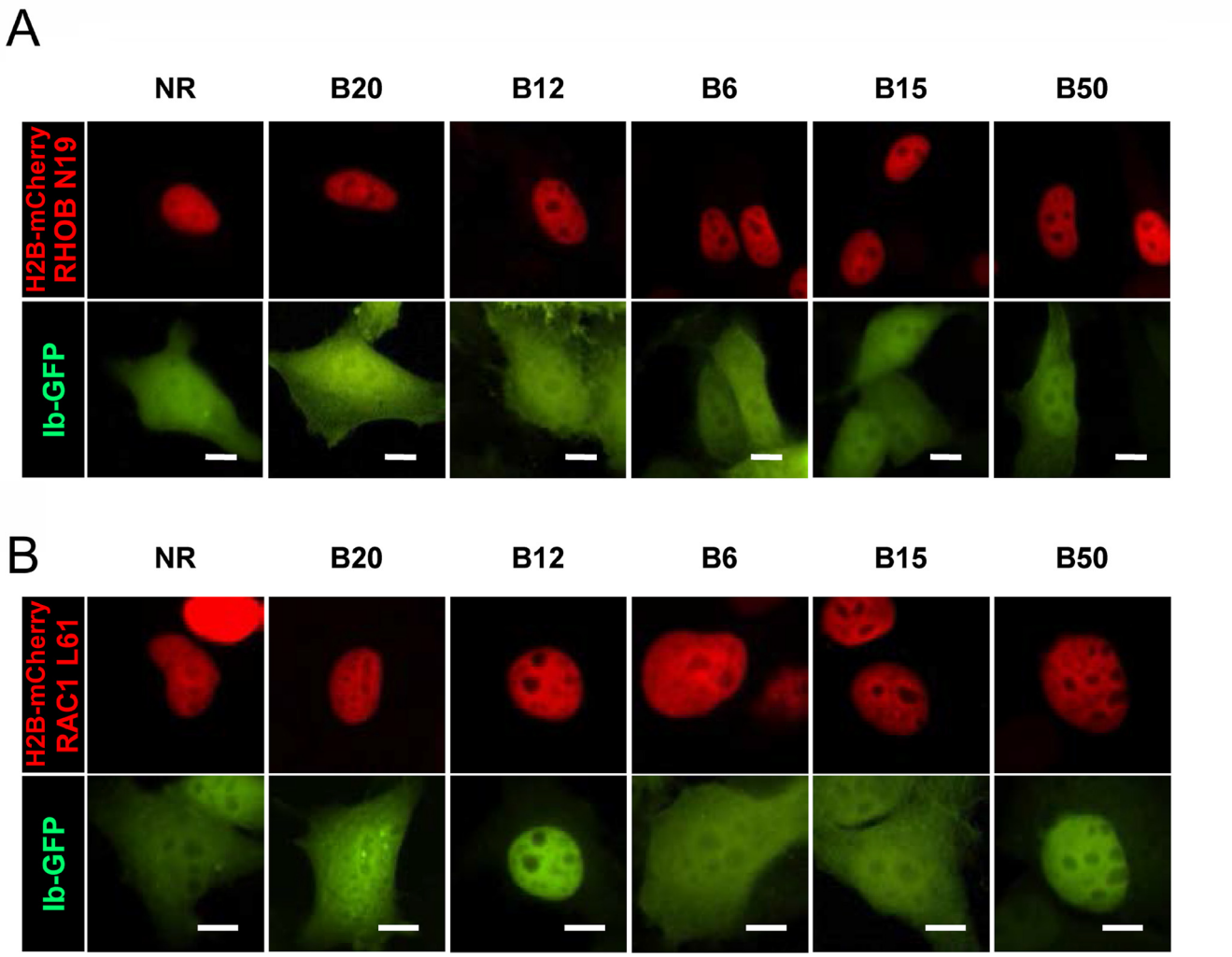

Figure S2: related to Figure 2. Ib intrabodies conformational selectivity confirmed by a nuclear localization assay of Ibs fused to GFP. Ib-GFP were co-transfected in HeLa S3 cells with the nuclear constructs HmRHOB N19 (A), or HmRAC1 L61 (B). None of the Ib-GFP was able to localize strictly into the nucleus when RHOB N19 was over-expressed in this sub-cellular compartment. Only Ib B12 and B50 re-localized into the nucleus when RAC1 L61 mutant was over-expressed (scale bars, 10 μm).

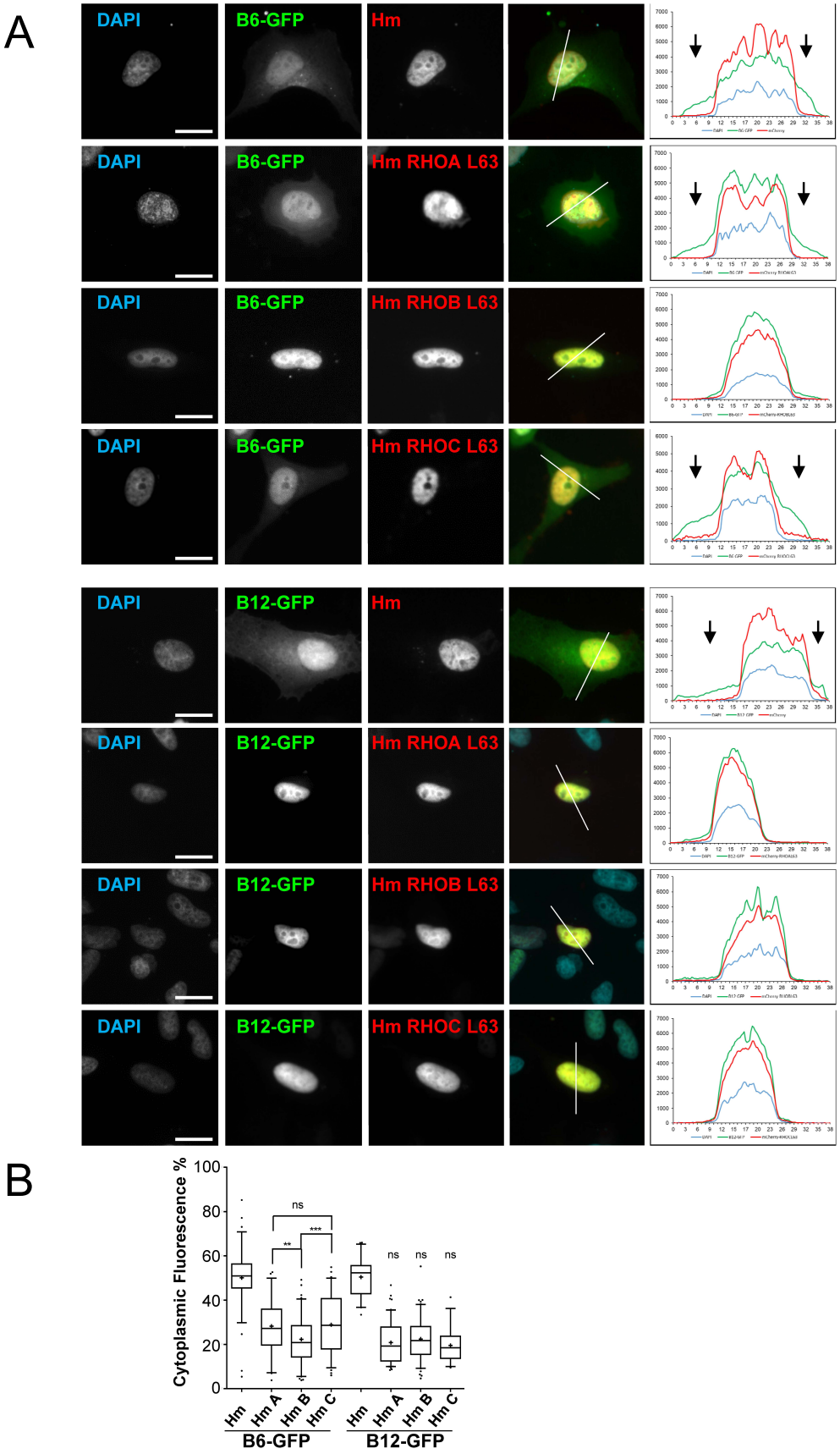

Figure S3: related to Figure 2. Ib intrabodies selectivity towards RHOA/B/C by a nuclear localization assay of Ib fused to GFP. (A) Ib-GFP were co-transfected in HeLa S3 cells with the nuclear constructs H2B-mCherry (Hm), H2B-mCherry-RHOA L63 (Hm RHOA L63 or also Hm A), H2B-mCherry-RHOB L63 (Hm RHOB L63 or also Hm B), or H2B-mCherry-RHOC L63 (Hm RHOC L63 or also Hm C). Representative cells and cut profile plots illustrate that B6-GFP was only strictly nuclear in cells displaying chromatin associated RHOB L63 but showed, with other constructs, some extra nuclear signal (arrows indicate cytoplasmic GFP signal) (scale bars, 20 µm). (B) Quantification of the extra-nuclear signal on transfected cells (n>100) is shown as the percentage of cytoplasmic fluorescence with, within the 5-95 percentile box plot, means as a + and median as a horizontal bar. Ns: non-significant, ** $P < 0.01$, *** $P < 0.001$.

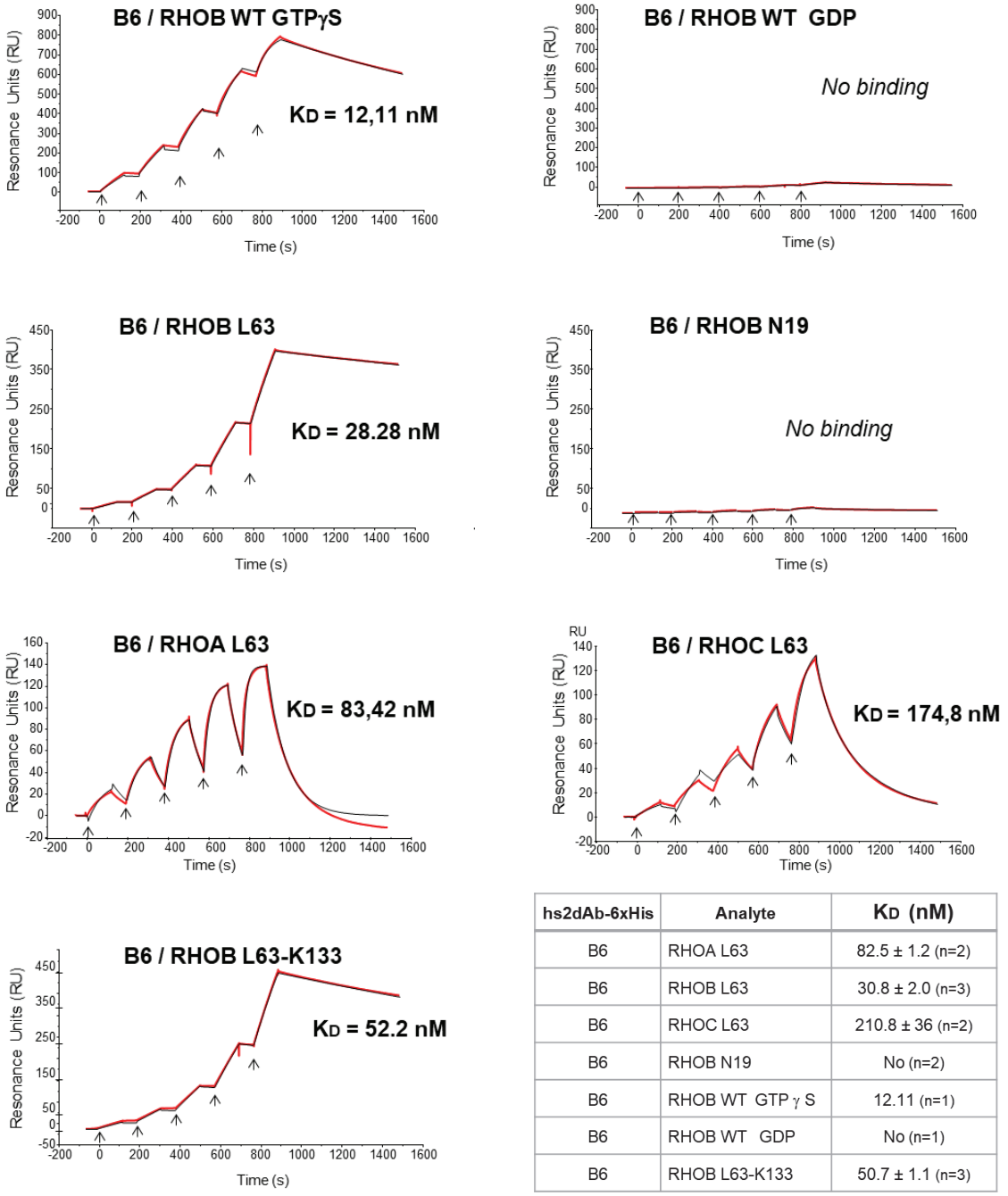

hs2dAb-6xHis	Analyte	KD (nM)
B6	RHOA L63	82.5 ± 1.2 (n=2)
B6	RHOB L63	30.8 ± 2.0 (n=3)
B6	RHOC L63	210.8 ± 36 (n=2)
B6	RHOB N19	No (n=2)
B6	RHOB WT GTP γ S	12.11 (n=1)
B6	RHOB WT GDP	No (n=1)
B6	RHOB L63-K133	50.7 ± 1.1 (n=3)

Figure S4: related to Figure 4. B6 nanobody affinity determination by SPR. Representative measurements of single cycle kinetics (SCK) analysis and a summary table of all KD values obtained for the B6 hs2dAb with various RHO variants as analytes (RHOB WT loaded with either GTP gamma S or GDP, RHOB L63, RHOB N19, RHOA L63, RHOC L63 and RHOB L63 K133). For each measurement, SCK analysis was simultaneously performed on immobilized B6-His6 on NTA sensorchip (250–300 RU), with five injections of purified RHO isoforms as analytes at 25 nM, 50 nM, 100 nM, 200 nM, and 400 nM. Analytes injections lasted for 200 sec each and were separated by 10 sec dissociation phases. Off-rate constant was calculated from an extended dissociation period of 10 min following the last injection according to the single cycle kinetics method. Each sensorgram (expressed in RUs as a function of time in seconds) represents a differential response where the response on an empty reference channel (Fc1) was subtracted. The red curves correspond to the data and the black curves represent the fit done by the BIAevaluation software.

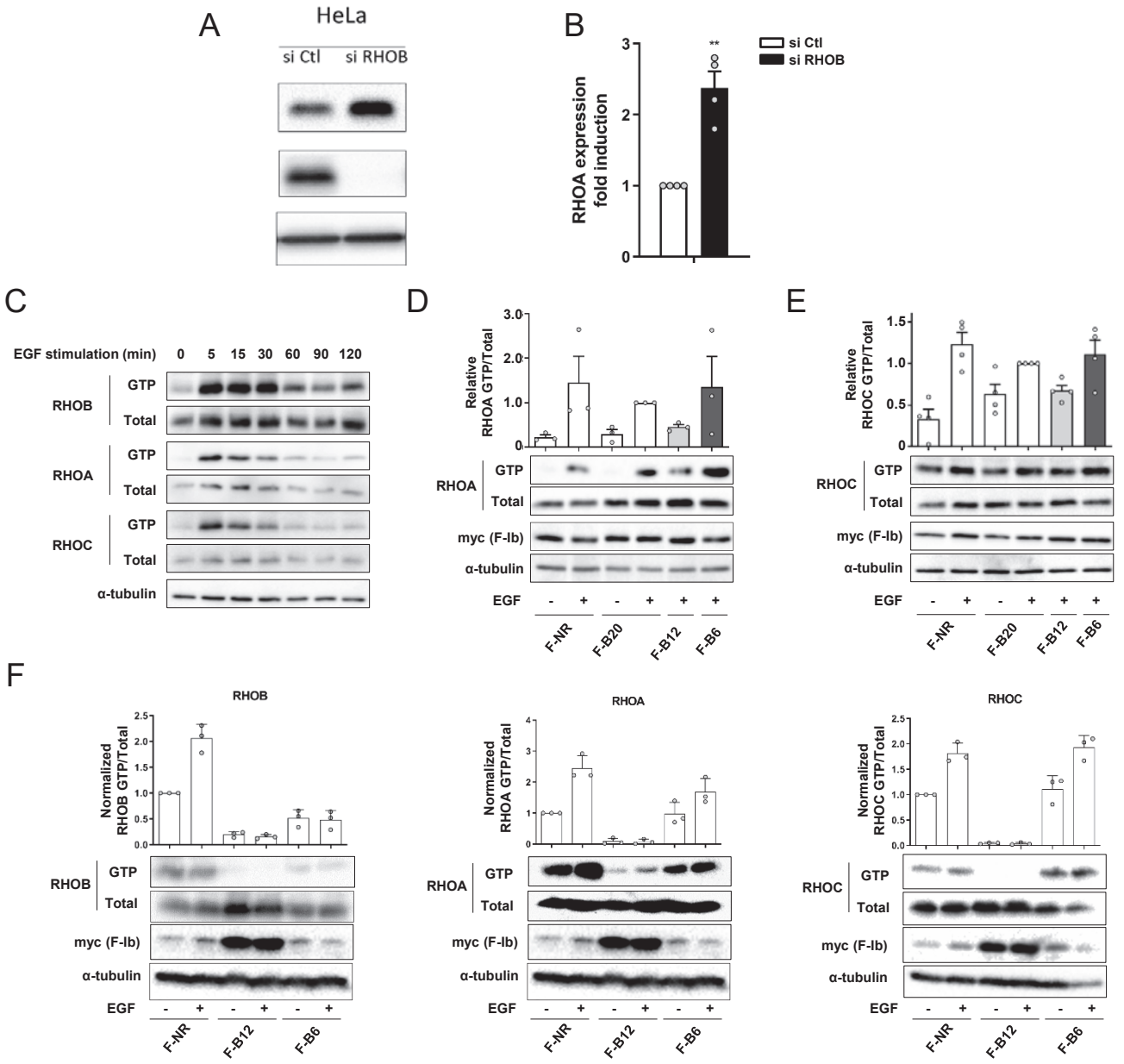

Figure S5: related to Figure 5. RHOB RNAi induction of RHOA and RHO activation knockdown upon EGF stimulation.

(A) Hela S3 transfected with control or RHOB siRNA smart pool showed upregulation of RHOA level in western. (B) Quantification of RHOA fold increase in context of RHOB loss. Normalized means ± SD are shown (n=4 biological repeats). ** $P < 0.01$.

(C) RHOB activation after an EGF treatment. HeLa S3 cells were transfected with F-NR control 48h including 24h of serum starvation. At 48h of transfection, cells were treated at an EGF concentration of 50 ng.mL-1 for indicated times. A GST-RBD pull-down was performed to monitor the RHO-GTP induction following this treatment. RHOB is activated within 5 min until 30 min and a second wave of activation is shown at 120 min. RHOA and RHOC are activated only between 5 and 30 min with a maximum at 5 min. (D&E) After 15 min of EGF treatment and 48h of cells transfection by F-Ib, RHOA-GTP (D) and RHOC-GTP (E) levels were analyzed. Unlike F-B12, F-B6 is not able to inhibit RHOA or RHOC activation following an EGF treatment compared to the negative control. Quantification is shown with normalized means ± SEM of at least three independent experiments. (F) Similar experiments (n=3 biological repeats) including the non-stimulated conditions for the F-B12 and the F-B6 show that the targeted protein degradation is very effective on both the basal and the activated fraction of RHOB for the F-B6 condition and for the three RHOs for the F-B12. No signal was detectable for RHOC-GTP in the F-B12 condition at the exposure time of the representative blot.

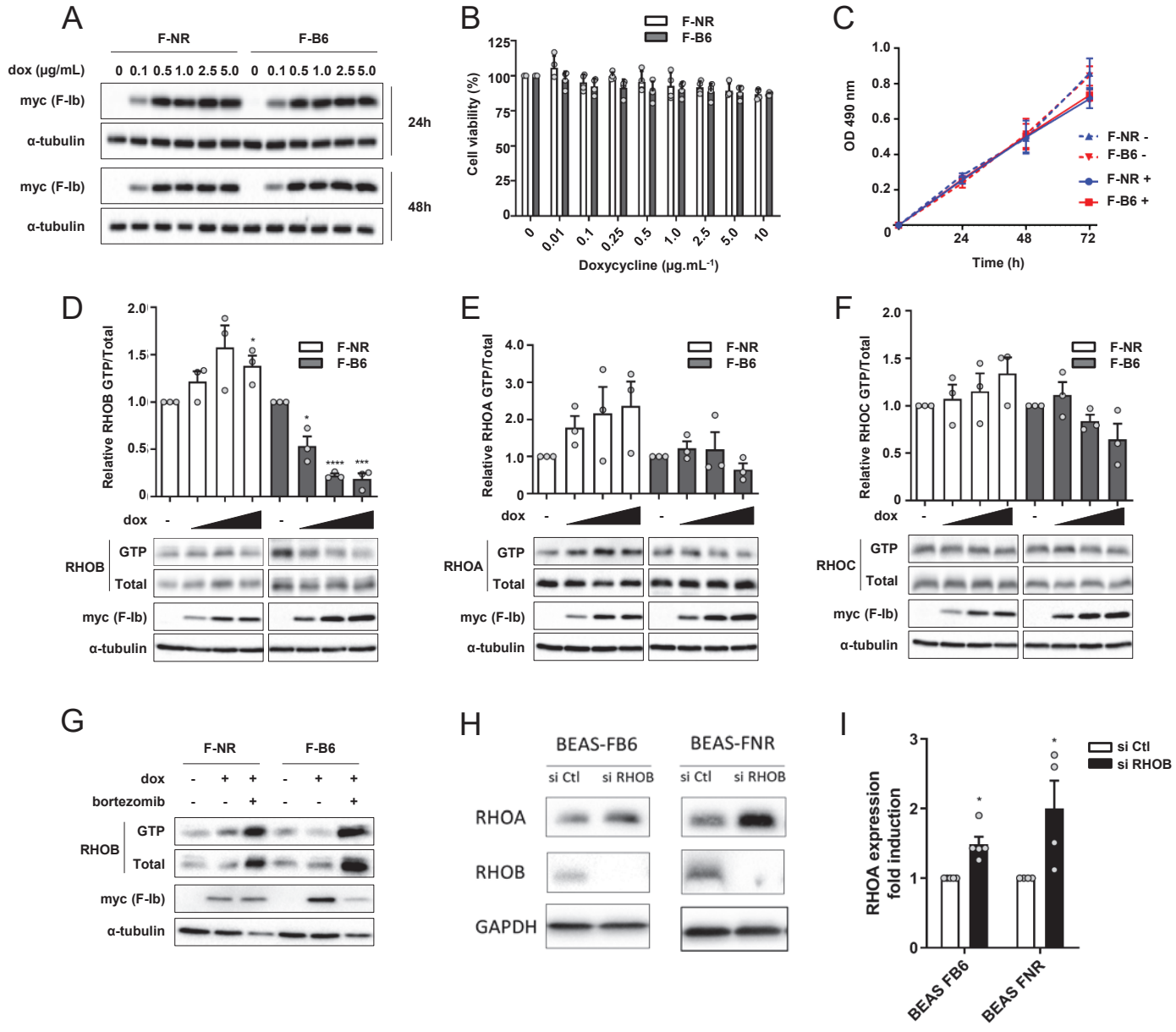

Figure S6: related to Figure 7. Characterization of the stable cell lines with tetracycline inducible (Tet-On) F-Ib expression. BEAS-2B cells were transduced with a F-Ib-IRES-BFP lentiviral vector including a tetracycline inducible (Tet-On) F-Ib expression. (A) F-NR and F-B6 cell lines were treated with an increased dose of doxycycline during 24h and 48h and the production of F-Ib was analyzed by western blot analyzes (Myc tag). The maximal expression of F-NR and F-B6 started at 48h after induction at 1 µg.mL^{-1}. (B) BEAS-2B cell viability was measured by a MTS assay incubating cells with increased doxycycline doses for 48h. No difference is visualized between F-NR and F-B6 for a dox dose. The relative viabilities normalized by the ones of no treatment (0 µg.mL^{-1}) were determined as means ± SD from four independent experiments. (C) A proliferation assay was performed at a dox dose of 1 µg.mL^{-1}. BEAS-2B cells were incubated with doxycycline for 24, 48 and 72h and proliferation was measured with a MTS assay. Proliferation is not modified when F-NR and F-B6 are produced by their respective cell lines. Data are means ± SD from three independent experiments. After 48h of F-Ib induction at various doxycycline concentrations (0, 0.1, 1 and 2.5 µg.mL^{-1}), RHO-GTP levels were followed and quantified with a GST-RBD pull-down, RHOB-GTP (D), RHOA-GTP (E) and RHOC-GTP (F). RHOB-GTP selectivity of F-B6 is still conserved and a dose response effect is shown for RHOB-GTP degradation. Data are normalized means ± SEM (n=3 biological repeats). * $P < 0.05$, *** $P < 0.001$, **** $P < 0.0001$. (G) RHOB-GTP degradation induced by F-B6 is rescued by the proteasome inhibitor bortezomib (1 µM). (H) BEAS-2B F-NR and BEAS-2B F-B6, in non-induced conditions, were transfected with control or RHOB siRNA smart pool and showed upregulation of RHOA level in western blot. (I) Quantification of RHOA fold increase in context of RHOB loss. Normalized means ± SD are shown (n= at least 4 biological repeats). * $P < 0.05$.

Table S1: related to Figure 4. Crystallography data collection, phasing, and refinement statistics.

Name	RHOB-GTP	RHOB-GTP/B6
PDB	6HXU	6SGE
Data collection	ID23-1 (ESRF)	ID29 (ESRF)
Wavelength (Å)	0.969	0.965
Space group	P 2 21 21	P 1 21 1
Unit cell	38.9 61.5 76.7	66.8 70.2 71.2 90 107.7 90
Resolution (Å)[a]	34.69 - 1.19 (1.233 - 1.19)	47.17 - 1.5 (1.554 - 1.5)
R_{meas} (%)[b]	0.02535 (0.1703)	0.0336 (0.4618)
CC* (%)[c]	1 (0.991)	1 (0.973)
Mean I/sigma(I)	20.63 (4.90)	20.06 (2.22)
Completeness (%)	98.65 (90.66)	0.95 (0.73)
Reflections, total	116433 (10003)	284589 (15398)
Reflections, unique	58942 (5349)	95400 (7264)
Multiplicity	2.0 (1.9)	3.0 (2.1)
R_{work} (%)[d]	0.1604 (0.1878)	0.1640 (0.2490)
R_{free} (%)[d]	0.1749 (0.2137)	0.1873 (0.2907)
Number of non-hydrogen atoms	1831	5626
macromolecules	1504	4880
water	293	678
ligands	34	68
Average B-factor (Å²)	20.3	18.71
Rmsd bond lengths (Å)	0.013	0.017
Rmsd bond angles (°)	1.32	1.53
Ramachandran favored (%)	98.33	97
Ramachandran allowed (%)	1.67	3

[a] Highest resolution shell is shown in parenthesis.

[b] $\text{Rmeas} = (\sum_{hkl} \sqrt{\frac{n}{n-1}} \sum_{i=1}^{n} |I_i(hkl) - \bar{I}(hkl)|) / \sum_{hkl} \sum_{i=1}^{n} I_i(hkl)$

[c] $\text{CC*} = \sqrt{2CC_{1/2}/(1 + CC_{1/2})}$

[d] $\text{Rwork} = \sum_{hkl}(|F_{obs}(hkl)| - |F_{calc}(hkl)|) / \sum_{hkl} |F_{obs}(hkl)|$ and Rfree is the R value for a test set of reflections consisting of a random 5% of the diffraction data not used in refinement.